UNIVERSITY OF
Southampton
Institute of Sound and
Vibration Research

ISVR Technical Memorandum

Lumped Parameter Model of the Organ of Corti

Marcos F. Simon Galvez and S.J. Elliott

ISVR Technical Memorandum No 1000

August 2013

SCIENTIFIC PUBLICATIONS BY THE ISVR

Technical Reports are published to promote timely dissemination of research results by ISVR personnel. This medium permits more detailed presentation than is usually acceptable for scientific journals. Responsibility for both the content and any opinions expressed rests entirely with the author(s).

Technical Memoranda are produced to enable the early or preliminary release of information by ISVR personnel where such release is deemed to the appropriate. Information contained in these memoranda may be incomplete, or form part of a continuing programme; this should be borne in mind when using or quoting from these documents.

Contract Reports are produced to record the results of scientific work carried out for sponsors, under contract. The ISVR treats these reports as confidential to sponsors and does not make them available for general circulation. Individual sponsors may, however, authorize subsequent release of the material.

UNIVERSITY OF SOUTHAMPTON

INSTITUTE OF SOUND AND VIBRATION RESEARCH

SIGNAL PROCESSING AND CONTROL GROUP

Lumped parameter model of the organ of Corti

by

Marcos F. Simón Gálvez and Stephen J. Elliott

Contents

List of Figures

List of Tables

List of Acronyms

BM basilar membrane

TM tectorial membrane

OHC outer hair cells

IHC inner hair cells

OC organ of Corti

RL reticular lamina

HPF high pass filter

IR impulse response

CP cochlear partition

FE finite elements

CF characteristic frequency

Abstract

Predictions of the active mechanical response in the guinea pig cochlea have been obtained from an elemental model, having an analytic formulation of the fluid coupling and a lumped parameter representation of the organ of Corti. The lumped parameter model is derived from the organ of Corti geometry and has three degrees of freedom, as used by Ramamoorthy *et al.* [1], whose values for the various mechanical parameters were used in the numerical simulation here. The coupled model has also been expressed in state space form, in order to assess its stability for different active feedback gains. The analytical model of the fluid coupling allows the far field and the near field components of to be accounted for separately, so that the difference between 1D and 2D fluid coupling can be investigated. It is found that in order to get reasonable agreement with the results of Ramamoorthy *et al.* [1], a reduced near field fluid coupling component has to be used, suggesting that the size of this component, which is controlled by the number of radial fluid modes they accounted for, was used as a tuning parameter in their work. A simplified model of the active feedback due to the outer hair cells is also described, which quantifies the electromechanical coupling coefficient used by various authors. Longitudinal electrical coupling has, however, been ignored in the present model, which might be the reason why the maximum active gain is about 5 dB less than that reported by Ramamoorthy *et al.* [1]. The present model reproduces the realistic difference between the active and passive basilar membrane responses obtained by these authors in both frequency and time domains.

1 Introduction

It is important to construct models of cochlear mechanics to test our understanding of the peripheral hearing system. Using an elemental approach, such models can conveniently be split into two parts, one concerned with fluid coupling and the other concerned with the dynamics of the organ of Corti. In this report, a lumped parameter model of the active OC is developed, which is physiologically reasonable, and its properties are discussed.

Although the OC combines bending and shear motion, this motion is translated into a single axis using the relations presented by Allen [2], and discussed by Elliott *et al.* [3, 4, 5]. The model presented here is based in a three degree of freedom system, in where the masses can be associated with the BM and the transverse and shear motion of the TM. Models using similar dynamics have been previously developed by Geisler *et al.*[6] and by Ramamoorthy *et al.*[1], however, these models use a feedfoward approach to the active pressure due to the OHC forces.

Although the full effect of 3D fluid coupling can be incorporated into the elemental formulation of the coupled cochlea, it is the near field component of the pressure that has a significant effect on the local OC dynamics. In order to understand the interplay between different elements of the OC dynamics, particularly when it is active, it is helpful to include the added mass due to the near fluid loading in the part of the model associated with the OC dynamics rather than in the fluid coupling part of the model. In fact, it is found that the results of Ramamoorthy *et al.*[1] are best reproduced with a fluid coupling having a diminished near fluid component of the fluid coupling, compared with the analytic value for this component.

In Section 2 the individual dynamic responses of the BM and TM are discussed. In order to provide a concrete example of the response of those components of the OC, numerical values of the various physical parameters are taken from the publications of the Michigan group[1], which have been chosen to represent a guinea pig cochlea. In Section 3 the equations of motion of the model are introduced, and Section 4 describes the distribution of parameters. The introduction of an active feedback loop into the organ of Corti dynamics is described in Section 5, and the coupled response described in Section 6. The results of simulations of the coupled response at various positions along the cochlea are given in Section 7, before conclusions are drawn in Section 8. A different distribution of cochlear chamber dimensions is also presented in Appendix A, which uses cochlear chambers with the dimensions found in a Guinea pig. Appendix B describes the extension of the state space formulation to include this three degree of freedom micromechanics model. Appendices C and D discuss the simplification that have been made to the electrical coupling.

2 BM and TM dynamics

Fig. 1a shows a cross section of the cochlea, including the main components of the OC. The arch of Corti is believed to pivot about its left bottom corner, which is attached to the BM and causes this to rotate as a more or less rigid body around this point. Similarly, the RL is believed to rotate about the top vertex of the arch of Corti. The TM and the RL are connected via the outer hair cells (OHC) and inner hair cells (IHC). The relative displacement of the OHC stereocilia is used in the model to recreate the force that simulates an active cochlea.

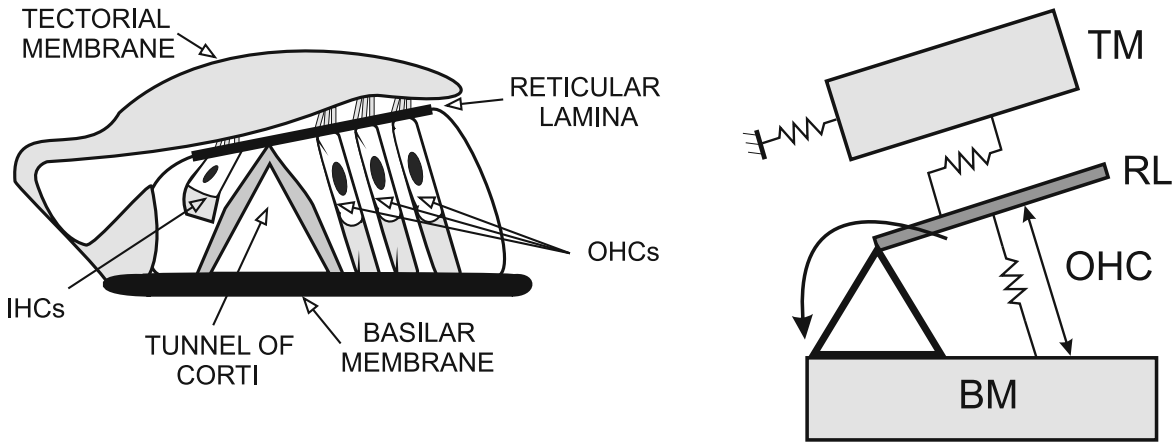

(a) **(b)**

Figure 1: Sketch and lumped parameter model of the OC.

In the passive cochlea, the OHC are not active, and these, together with the TM mainly act as mass loading in the BM. The passive response of the OC can thus reasonably well represented as a single degree of freedom system. In order to recreate the active behaviour that leads to a greater frequency selectivity, it is needed to include one or two extra masses to create a higher order resonant system.

Fig. 1b shows how the OC can be transformed into a lumped parameter model, where motion is assumed to be present radially (shear motion) and transversally (bending motion). This shear motion is then transformed into an equivalent bending motion, which can be performed by assuming that the RL pivots around the top corner of the tunnel of Corti. This geometry change was introduced by Allen in 1980 who assumed that BM and TM move parallel to one another. For the case of the model presented here, this parallel motion occurs between the TM and RL.

As the two right angle triangles shown in Fig. 2 are similar, the angle of rotation θ is also similar, which leads to the relation

$$\sin\theta = \frac{w}{l} \text{ and } \sin\theta = \frac{\Delta}{h}, \tag{2.1}$$

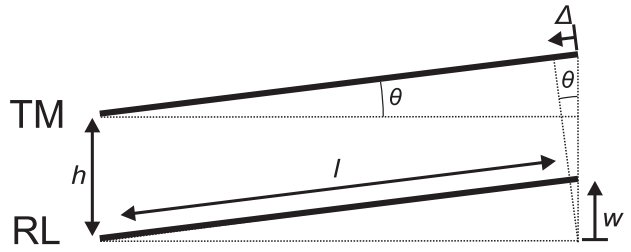

Figure 2: Relation between shear and bending displacement on the TM.

so that

$$\frac{\Delta}{w} = g = \frac{h}{l}, \tag{2.2}$$

where g is known as the *shear gain* and depends on the geometry of the OC. Using this relation, it is possible to relate the transverse motion to the shear motion, i.e,

$$w_{RL} = \frac{\Delta_{RL}}{g}. \tag{2.3}$$

As can be observed in Fig. 3b, the radial motion of the TM due to radial pressure p_{SR} is governed by the equation

$$p_{SR} = k'_4 \Delta_{TM} + s^2 m'_3 \Delta_{TM}, \tag{2.4}$$

where k'_4 and m'_3 are the physical shear stiffnesses and masses of the TM. This pressure is generated by the relative radial displacements of TM and RL

$$p_{SR} = k'_3(\Delta_{TM} - \Delta_{RL}). \tag{2.5}$$

We can define an equivalent transverse pressure acting on the RL due to the TM, p_{ST}. Since the work per unit area done by the RL in the shear direction, $\Delta_{RL} p_{SR}$, must be equal to that in the equivalent transverse direction, $w_{RL} p_{ST}$, then using Eq. 2.3, the equivalent transverse pressure can be related to the shear pressure by $p_{ST} = g p_{SR}$. Since h is approximately equal to 1, a value of 1 is used for g here, so that the equivalent transverse pressure is equal to the physical radial pressure. Using this relation and the relation of Eq. 2.2, p_{ST} can be defined as

$$p_{ST} = g^2(k'_4 w_{TM} + s^2 m'_3 w_{TM}), \tag{2.6}$$

which can be written as

$$p_{ST} = (k_4 + s^2 m_3) w_{TM}, \tag{2.7}$$

where $k_4 = g^2 k'_4$ and $m_3 = g^2 m'_3$ refer to the equivalent transverse stiffness and mass. Similarly, the equation describing the radial stiffness of the cilia, Eq. 2.5 can be transformed into transverse motion to give

$$p_{ST} = g^2 k'_3(w_{BM} - w_{TM}), \tag{2.8}$$

or

$$p_{ST} = k_3(w_{BM} - w_{TM}), \tag{2.9}$$

where $k_3 = g^2 k'_3$. The transverse force required to drive the RL must, in addition to p_{ST}, also include that required to overcome the transverse inertia of the RL and TM masses, m_2

and the equivalent stiffnesses due to the RL rotation, k_5. By the use of these relationships, the OC model is transformed from having motion in two axes, as shown in Fig. 3a to a model with motion in only one axis, as in Fig. 3b, where p_A is the pressure difference due to the fluid in the cochlear chambers.

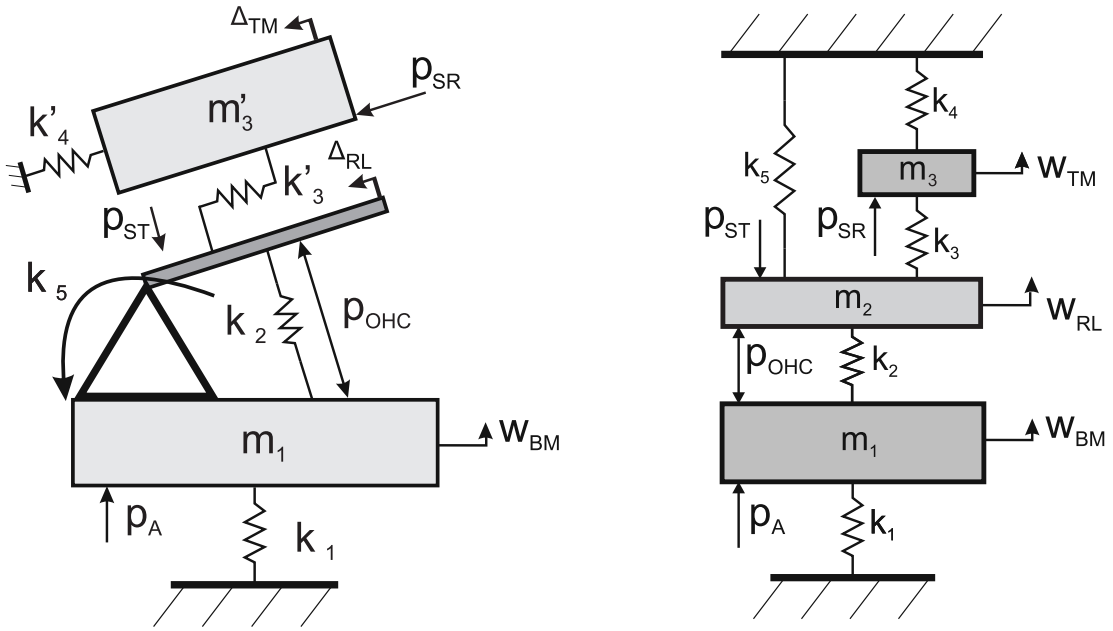

(a) Shear and transversal motion. **(b)** With motion in only one axis.

Figure 3: Lumped parameter model of the OC. The damping associated with each stiffness is not shown for notational convenience.

3 Dynamics of the organ of Corti

Three equations of motion are introduced for the system of Fig. 3b,

$$p_A - p_{OHC} = s^2 m_1 w_{BM} + k_1 w_{BM} + k_2(w_{BM} - w_{RL}), \tag{3.1}$$

$$p_{OHC} = s^2 m_2 w_{RL} + k_2(w_{RL} - w_{BM}) + k_3(w_{RL} - w_{TM}) + k_5 w_{RL}, \tag{3.2}$$

$$s^2 m_3 w_{TM} + k_3(w_{TM} - w_{RL}) + k_4 w_{TM} = 0, \tag{3.3}$$

where m_1 represents the mass of the BM and w_{BM} its displacement, m_2 represents the physical mass of the TM and w_{TM} its transverse displacement and m_3 represents the transformed mass of the TM due to its radial motion and w_{TM} its equivalent transversal motion as discussed in Section 2. Each stiffness is also complex and can be written as $k+sc$ where k is the real stiffness and c the associated damping. The receptance for each mass when these are driven by p_A and p_{OHC}, are obtained here by performing using Gaussian elimination.

The displacement of the TM, w_{TM}, is specified as a function of that of the RL, w_{RL}, by using Eq. 3.3. A transfer function denoted $T_{TM/RL}$ is created

$$(s^2 m_3 + k_3 + k_4) w_{TM} - k_3 w_{RL} = 0 \rightarrow \frac{w_{TM}}{w_{RL}} = T_{TM/RL} = \frac{k_3}{s^2 m_3 + k_3 + k_4}, \tag{3.4}$$

which is referred to as the *shear transfer function*[1]. The same operation is performed with Eq. 3.2, which combined with Eq. 3.4 allows us to express w_{RL} as a function of the displacements of the BM and TM, w_{BM} and w_{RL} respectively. This transfer function is denoted as $T_{RL/(BM+TM)}$

$$(s^2m_2 + k_2 + k_3 + k_5)w_{RL} - k_3w_{TM} - k_2w_{BM} = 0,$$

$$\left[(s^2m_2 + k_2 + k_3 + k_5) - k_3T_{TM/RL}\right] w_{RL} = k_2w_{BM}. \tag{3.5}$$

Hence

$$\frac{w_{RL}}{w_{BM} + w_{TM}} = k_2T_{RL/(BM+TM)} = k_2\left[(s^2m_2 + k_2 + k_3 + k_5) - k_3T_{TM/RL}\right]^{-1}. \tag{3.6}$$

A final relationship is introduced to relate w_{BM} with w_{RL}. This is denominated as $T_{BM/RL}$ and is obtained directly by equalling to 0 Eq. 3.1

$$(s^2m_1 + k_1 + k_2)w_{BM} - k_2w_{RL} = 0,$$

$$T_{BM/RL} = \frac{w_{BM}}{w_{RL}} = \frac{k_2}{s^2m_1 + k_1 + k_2}. \tag{3.7}$$

By using these three relationships, the receptance of the three masses of the micromechanical model with respect to p_A and p_{OHC} can be obtained.

The receptance of the BM respect to the acoustic driving pressure, $G_{BA} = w_{BM}/p_A$, is obtained by using Eq. 3.5 and expressing w_{RL} as a function of w_{BM}

$$p_A = (s^2m_1 + k_1 + k_2)w_{BM} - k_2w_{RL} = (s^2m_1 + k_1 + k_2 - k_2^2T_{RL/(BM+TM)})w_{BM},$$

$$G_{BA} = \frac{w_{BM}}{p_A} = \frac{1}{s^2m_1 + k_1 + k_2(1 - k_2T_{RL/(BM+TM)})}. \tag{3.8}$$

Similarly, the receptance of the BM when driven by the active pressure, $G_{BO} = w_{BM}/p_{OHC}$, is obtained by equalling Eq. 3.1 and Eq. 3.2 to p_{OHC} and expressing w_{RL} and w_{RL} displacements as a function of w_{BM}. When including the active pressure, w_{RL} is related to w_{BM} as

$$\left[(s^2m_2 + k_2 + k_3 + k_5) - k_3T_{TM/RL}\right] w_{RL} = p_{OHC} + k_2w_{BM},$$

$$w_{RL}T^{-1}_{RL/(BM+TM)} = p_{OHC} + k_2w_{BM},$$

$$w_{RL} = k_2T_{RL/(BM+TM)}w_{BM} + T_{RL/(BM+TM)}p_{OHC}.$$

So, for Eq. 3.1

$$(s^2m_1 + k_1 + k_2)w_{BM} - k_2\left(k_2T_{RL/(BM+TM)}w_{BM} + T_{RL/(BM+TM)}p_{OHC}\right) = -p_{OHC},$$

$$\left(s^2m_1 + k_1 + k_2 - k_2^2T_{RL/(BM+TM)}\right) w_{BM} = p_{OHC}\left(-1 + k_2T_{RL/(BM+TM)}\right),$$

$$G_{BO} = \frac{w_{BM}}{p_{OHC}} = \frac{-1 + k_2T_{RL/(BM+TM)}}{s^2m_1 + k_1 + k_2 - k_2^2T_{RL/(BM+TM)}}. \tag{3.9}$$

Other displacement of interest is that given by the relative displacements of RL and TM, $w_{RL} - w_{TM}$, which represents the displacement that the OHC stereocillia overcome, w_{ST}.

[1]This denomination was first introduced by Allen[2] to relate bending displacements of TM and BM.

First we introduce the stereocillia displacement for a given acoustic pressure input at the BM, $G_{SA} = w_{ST}/p_A$. For obtaining this displacement, it is needed first to express w_{RL} as a function of p_A.

$$w_{RL}\left((s^2m_1 + k_1 + k_2)\frac{T^{-1}_{RL/(BM+TM)}}{k_2} - k_2\right) = p_A,$$

$$\frac{w_{RL}}{p_A} = \left((s^2m_1 + k_1 + k_2)\frac{T^{-1}_{RL/(BM+TM)}}{k_2} - k_2\right)^{-1}. \tag{3.10}$$

By using Eq. 3.4 w_{TM} is expressed as a function of w_{RL},

$$w_{ST} = w_{RL} - w_{TM} = w_{RL} - T_{TM/RL}w_{RL} = (1 - T_{TM/RL})w_{RL}. \tag{3.11}$$

So that if Eq. 3.10 and Eq. 3.11 are combined

$$G_{SA} = \frac{w_{ST}}{p_A} = (1 - T_{TM/RL})\left((s^2m_1 + k_1 + k_2)\frac{T^{-1}_{RL/(BM+TM)}}{k_2} - k_2\right)^{-1}. \tag{3.12}$$

The last receptance of interest is the one that relates the displacement of the stereocillia due to the active pressure, $G_{SO} = w_{ST}/p_{OHC}$. This quantity is obtained by expressing Eq. 3.1 and 3.2 as a function of w_{RL} and p_{OHC}.

For Eq. 3.1

$$(s^2m_1+k_1+k_2)w_{BM}-k_2w_{RL} = -p_{OHC} \rightarrow w_{BM} = (k_2w_{RL}-p_{OHC})(s^2m_1+k_1+k_2)^{-1}. \tag{3.13}$$

Eq. 3.13 is now combined onto Eq. 3.2

$$w_{RL}T_{RL/(BM+TM)} = p_{OHC} + k_2w_{BM},$$

$$w_{RL}T_{RL/(BM+TM)} = p_{OHC} + k_2(k_2w_{RL} - p_{OHC})(s^2m_1 + k_1 + k_2)^{-1},$$

$$\left(T_{RL/(BM+TM)} + \frac{k_2^2}{s^2m_1 + k_1 + k_2}\right)w_{RL} = \left(1 - \frac{k_2}{s^2m_1 + k_1 + k_2}\right)p_{OHC},$$

which is reduced by using, $T_{BM/RL}$, Eq. 3.7

$$\left(T_{RL/(BM+TM)} + k_2T_{BM/RL}\right)w_{RL} = \left(1 - T_{BM/RL}\right)p_{OHC},$$

so that

$$\frac{w_{RL}}{p_{OHC}} = \frac{1 - T_{BM/RL}}{T_{RL/(BM+TM)} + k_2T_{BM/RL}}, \tag{3.14}$$

which if combined with Eq. 3.11 gives G_{SO}

$$G_{SO} = \frac{w_{ST}}{p_{OHC}} = \left(1 - T_{TM/RL}\right)\frac{1 - T_{BM/RL}}{T_{RL/(BM+TM)} + k_2T_{BM/RL}}. \tag{3.15}$$

In Section 7 is presented a detailed study of the frequency response of each of these receptances, using the parameters described in Section 4.

4 Distribution of parameters

In order to understand the dynamic behaviour of the OC model above at different positions along the cochlea, a distribution of parameter values has to be assumed. Whereas the values of stiffnesses and damping and TM mass can be taken from the literature[1, 7], the effective value of the BM mass is affected by fluid loading. If 1D fluid coupling is assumed, in order to help understand the properties of the OC dynamics[8, 9] the effective value of the BM mass must be increased to take the near field component of the fluid coupling into account[10, 11, 7]. In this case the mass per unit area can be expressed as

$$m_1 = m_{BM} + m_F, \tag{4.1}$$

where m_{BM} is the physical mass of the BM given by $\rho_{BM} h_{BM}$, being ρ_{BM} the BM density and h_{BM} its physical thickness, which decreases from 7 μm to 1.7 μm along the length of the cochlea[1]. m_F is the equivalent mass due to 3D fluid loading, given by $\rho_F T$, where T represents the effective thickness of the BM due to fluid loading, and is given by a function of the BM geometry within the cochlea by Eq 6.14. According with the assumptions of Ramamoorthy et al. [1] the BM width expanses linearly from 80 μm at the base to 200 μm at the apex, being the BM placed *centrally* in the fluid chambers, which have a constant width and height of 1 mm each, then T can be calculated to be 0.07 μm at the base to 0.14μm at the apex. If the BM is assumed to be placed on one side of the cochlear partition, rather than in the centre, the near fluid pressure, and the T, is increased by a factor of two [7]. If the physical weight of the BM and T are added, the final distribution of effective BM mass increases linearly from 0.08 Kgm^{-2} at the base to 0.14 Kgm^{-2} at the apex[2].

Ramamoorthy et al. [1] assume that the BM vibrates with a single mode shape in the radial direction, and coupled into the fluid with a finite number of radial fluid modes. From their Fig. 18, it would appear that 3 radial modes are typically accounted for in the fluid, although the results seem to be significantly different if 5 radial modes are included and it is not clear how many modes are necessary to get the model series for the fluid pressure to converge. In an earlier discussion of this description of the fluid coupling [12], it is explained how the transverse variation in the fluid pressure is accounted for with a simplified finite element formulation with piecewise linear shape functions. It is noted by these authors that it was necessary to account for 20 fluid radial modes in order to get convergence. It would thus appear that Ramamoorthy et al. [1] uses the number of radial modes accounted for in their model as a tuning parameter, perhaps to best match their coupled frequency responses with experimental results, rather than selecting a large enough number of modes to ensure convergence of the model they were using of fluid coupling. It has been shown by Ni [13] that the equivalent BM mass due to the fluid loading is rather sensitive to the number of fluid elements used in a 3D finite elements (FE) model of fluid coupling. It is thus difficult to exactly replicate the effective BM mass used in [1]. If however, the BM mass derived above is used with their BM stiffness, as corrected by Li [14], then the range of BM natural frequencies is from about 60 kHz at the base to 300 kHz at the apex, in reasonable agreement with that expected for a Guinea pig [15, 16].

The parameters used in the final version of the model presented here are listed in Table 1, together with indications of how and where they have been derived from. Note that for k_{OHC} the value used is twice the original value given by Ramamoorthy *et al.*, which are

[2]See comments of Section. 6.4

$6.08 \cdot 10^3$ Nm^{-2}. The values for the OHC stiffness *in vivo* are not known exactly, and a stiffness twice the original one has been used as it has shown to provide better coupled responses. The values used here are normalized by the area of each element, so that the input quantity to the model is the acoustic pressure that drives the BM and not a force, as in the model of Ramamoorthy *et al.*[1]. The spatial distributions for mass, stiffnesses, damping and natural frequencies can be observed in Figures 4 and 6.

The three degree of freedom OC model will have three modes, whose natural frequencies will, in general, depend on the values of all the masses and stiffneses. Since m_1, with near field fluid loading, is significantly larger than m_2 and m_3, however, the modes are mainly associated with different parts of the model and simplified approximate values of the natural frequencies can be calculated, as

$$f_{RL}(x) = \frac{1}{2\pi}\sqrt{\frac{k_2(x) + k_4(x) + k_5(x)}{m_2(x) + m_3(x)}}. \tag{4.2}$$

$$f_{BM}(x) = \frac{1}{2\pi}\sqrt{\frac{k_1(x)}{m_1(x)}}, \tag{4.3}$$

$$f_{TM}(x) = \frac{1}{2\pi}\sqrt{\frac{2k_3(x) + k_4(x) + k_5(x)}{m_3(x)}}, \tag{4.4}$$

If k_1, k_3 and k_4, are assumed to have an associated damper, the isolated damping ratios associated to each mass can be calculated as

$$\zeta_{RL}(x) = \frac{c_3(x)}{2m_2(x)\omega_{RL}(x)} \tag{4.5}$$

$$\zeta_{BM}(x) = \frac{c_1(x)}{2m_1\omega_{BM}(x)} \tag{4.6}$$

$$\zeta_{TM}(x) = \frac{c_3(x) + c_4(x)}{2m_3(x)\omega_{TM}(x)} \tag{4.7}$$

The relative amplitude and phase of the motions of m_1, m_2 and m_3 for each mode can be observed in Fig. 5, assuming parameters for $x = 5.75$ mm and excitation at each natural frequency. whilst that Fig. 6 shows the natural frequencies as a function of position obtained from a full analysis of the three degree of freedom system and the approximations above together with their damping ratios.

Table 1: Micromechanical parameters (upper table) and geometrical data (lower table) for the model.

Element	Original value	Original units	Conversion	Value	Units	Source
k_1	$8.40 \cdot 10^5 (h/h_0)^3 (b_0/b)^4$	Nm^{-2}	$k_1/b_{TM}^{(x)}$	$8.40 \cdot 10^5 (h/h_0)^3 (b_0/b)^4$	Nm^{-3}	Modified corrections from Li.[14], K_{BM}
k_2	$2 \cdot 6.08 \cdot 10^3 e^{-325x}$	Nm^{-2}	$k_2/b_{BM}^{(x)}$	$2 \cdot 6.08 \cdot 10^3 e^{-325x}/b_{BM}^{(x)}$	Nm^{-3}	Corrections from Li[14] ,K_{OHC}
k_3	$3.42 \cdot 10^4 e^{-325x}$	Nm^{-2}	$k_3/b_{BM}^{(x)}$	$3.42 \cdot 10^9 e^{-325x}/b_{BM}^{(x)}$	Nm^{-3}	Ref. [1] ,K_{HB}
k_4	$6.00 \cdot 10^3 e^{-220x}$	Nm^{-2}	$k_4/b_{BM}^{(x)}$	$6.00 \cdot 10^9 e^{-220x}/b_{BM}^{(x)}$	Nm^{-3}	Ref. [1], K_{TMs}
k_5	$7.60 \cdot 10^3 e^{-325x}$	Nm^{-2}	$k_5/b_{BM}^{(x)}$	$7.60 \cdot 10^9 e^{-325x}/b_{BM}^{(x)}$	Nm^{-3}	Ref.[1], K_{RL}
m_1	$0.007_{\text{(base) to}}\ 0.001_{\text{ (apex)}}$	kgm^{-2}	$m_{BM} + m_F$	$0.08_{\text{(base) to}}\ 0.14_{\text{ (apex)}}$	kgm^{-2}	Estimated from Ref. [1, 7], M_{BM}
m_2	$0.015e^{50x}$	kgm^{-1}	$m_2/b_{BM}^{(x)}$	$0.015e^{50x}/b_{BM}^{(x)}$	kgm^{-2}	Adjusted manually
m_3	gm_2			$0.015e^{50x}/b_{BM}^{(x)}$	kgm^{-2}	From [1], assumed g
c_1	0.10	Nsm^{-2}	$c_1/b_{BM}^{(x)}$	$0.10 \cdot 10^3/b_{BM}^{(x)}$	Nsm^{-3}	Corrections from Li[14], C_{BM}
c_2				0.00	Nsm^{-3}	
c_3	0.024	Nsm^{-2}	$c_3/b_{BM}^{(x)}$	$0.024 \cdot 10^3/b_{BM}^{(x)}$	Nsm^{-3}	Ref. [1], C_{TMs}
c_4	0.05	Nsm^{-2}	$c_4/b_{BM}^{(x)}$	$0.05 \cdot 10^3/b_{BM}^{(x)}$	Nsm^{-3}	Ref. [1], C_{TMs}
c_5				0.00	Nsm^{-3}	

Property	Value	Source
H	1 mm	Ref. [1]
W	1 mm	Ref. [1]
$b_{BM}^{(x)}$	$80_{\text{(base) to}}\ 200\ \mu\mathrm{m}_{\text{ (apex)}}$	Ref. [1]
$h_{BM}^{(x)}$	$7_{\text{(base) to}}\ 1.7\ \mu\mathrm{m}_{\text{ (apex)}}$	Ref. [1]

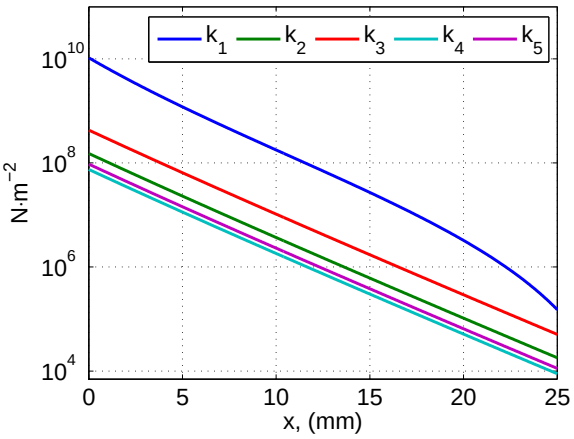

(a) Stiffnesses

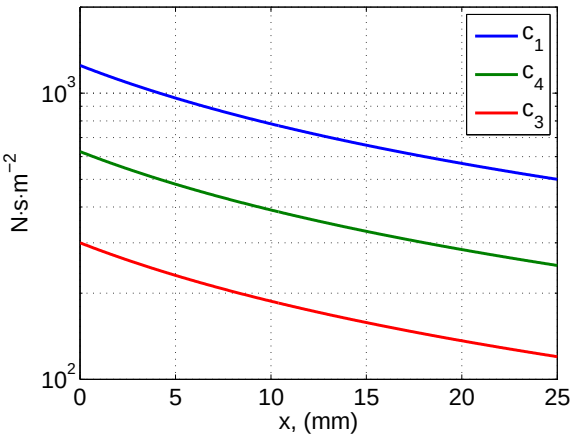

(b) Dampers

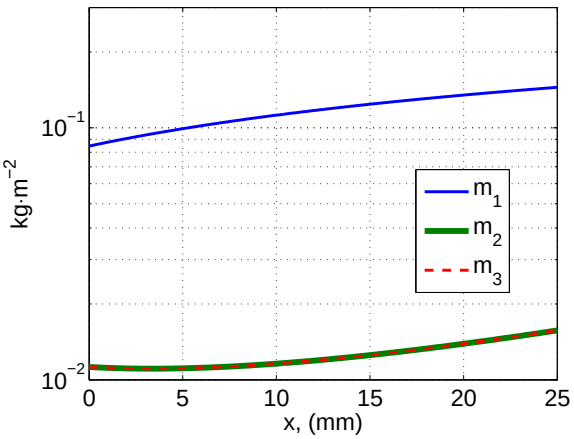

(c) Masses

Figure 4: Values of the parameters used in the model plotted against frequency.

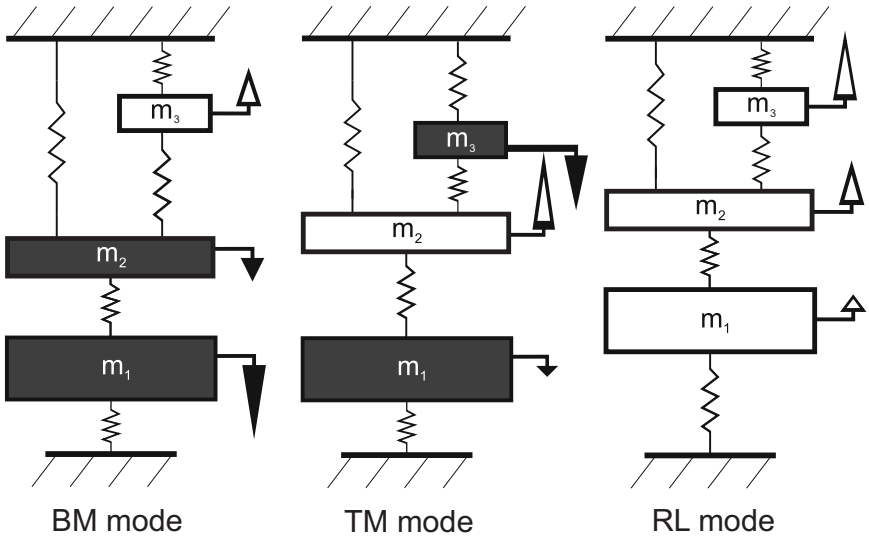

Figure 5: Relative phase of each of the observed modes of vibration of the OC. From left to right:
1) "BM mode", where the BM moves to a much greater extent than the RL or the BM.
2) "TM mode", where the motion of m_2 and m_3, representing the transverse and shear motion of the RL and TM, are out of phase and large compared with that of the BM.
3) "RL mode", where the motion of m_2 and m_3 are in phase but large compared with that of the BM.

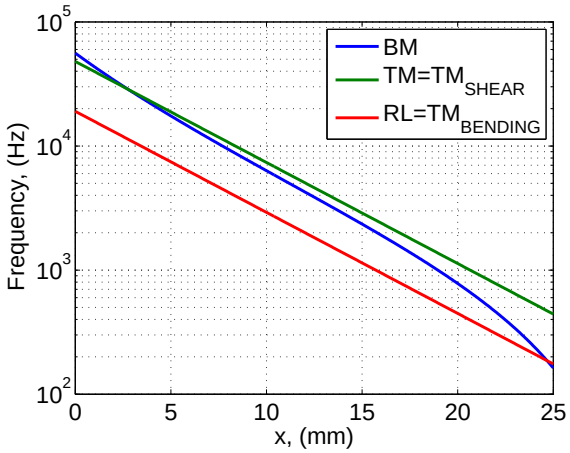

(a) Coupled system

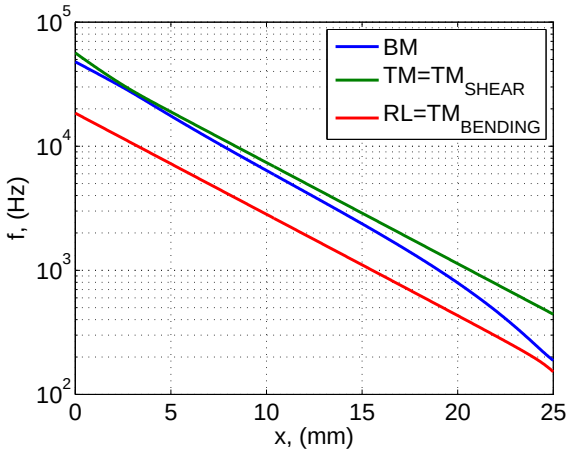

(b) Estimated based in isolated masses (Eqs. 4.2, 4.3 and 4.4).

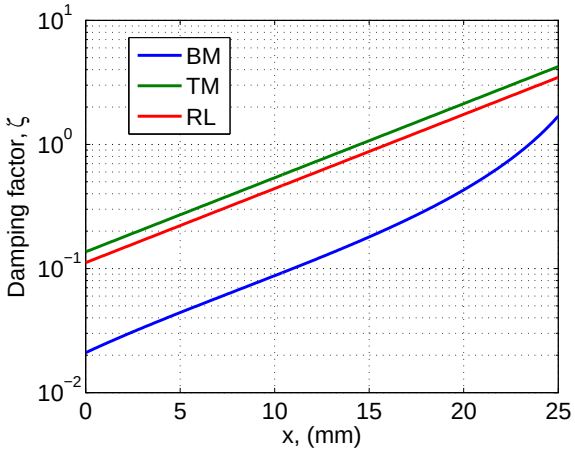

(c) Estimated based in isolated masses (Eqs. 4.5, 4.6 and 4.7).

Figure 6: Natural frequencies and damping factors of the BM, TM and RL using the parameters of Table. 1.

5 Active model of the organ of Corti

5.1 Formulation

The active response of the OC is introduced in the model of Fig. 3b by including a feedback loop whereby the control pressure, p_{OHC} is related to the shear displacement of the stereocillia, w_{ST}. The passive response of the OC is indicated as the responses inside the box in Fig. 7, in terms of the displacements of the BM, w_{BM}, and the shear displacement of the stereocillia between the RL and the TM, w_{ST}, in response to either the acoustic pressure along on the BM, p_A, and the pressure due to the OHC, p_{OHC}. p_{OHC} is then assumed to be driven by w_{ST} via the feedback response H.

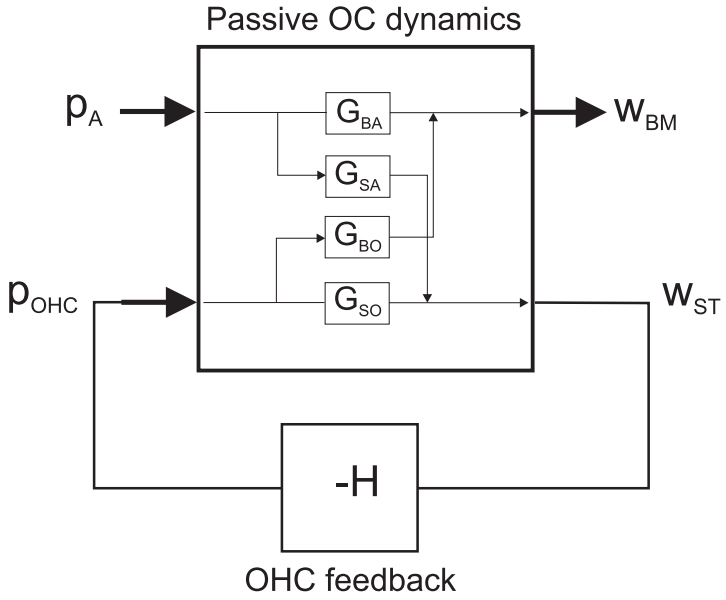

Figure 7: Block diagram of the active amplification that takes place in the OC model of Fig. 3b.

A set of equations for w_{BM} and w_{ST} can be obtained according to the block diagrams of Fig. 7, for the case of the open loop

$$w_{BM} = G_{BA}p_A + G_{BO}p_{OHC}, \tag{5.1}$$

$$w_{ST} = G_{SA}p_A + G_{SO}p_{OHC}. \tag{5.2}$$

The closed loop response can be derivated from these equations and the block diagram of Fig. 7. Given that

$$p_{OHC} = -Hw_{ST}, \tag{5.3}$$

hence

$$p_{OHC} = -H\left(G_{SA}p_A + G_{SO}p_{OHC}\right) \rightarrow p_{OHC} = \frac{-G_{SA}}{1 + G_{SO}H}p_A. \tag{5.4}$$

So that the closed loop displacement of the BM is given as

$$w_{BM} = \left(G_{BA} - G_{BO}\frac{HG_{SA}}{1 + G_{SO}H}\right)p_A, \tag{5.5}$$

and hence the closed loop mobility as

$$Y_{BM} = \frac{sw_{BM}}{p_A} = s\left(G_{BA} - G_{BO}\frac{HG_{SA}}{1 + G_{SO}H}\right), \tag{5.6}$$

where H represents a suitable controller as the one described in Appendix C, which can be written such as

$$H(j\omega) = \frac{\gamma g_H}{1 + \frac{j\omega}{\omega_{OHC}}}. \tag{5.7}$$

6 Coupled model of the cochlea

6.1 Elemental formulation

The cochlea can be modelled as a set of N micromechanical elements, being each of them tuned to a different resonant frequency depending on its position along the cochlea, and coupled through the inertia of the fluid in the chambers. For the case of the simulations presented, these have been calculated using $N = 1024$ elements. The elements in the cochlea are assumed to be equally spaced, as shown in Fig. 8.

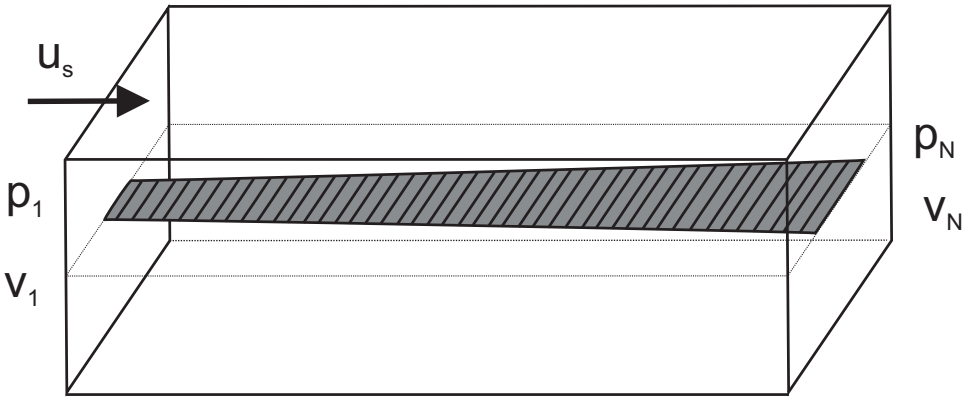

Figure 8: *Long wave* macromechanical model of the cochlea. Each slice represents one from a total of N micromechanical elements as the one of Fig. 3b.

We can define vectors of complex pressures and velocities at a single frequency at the position of each micromechanical element, $\mathbf{p}$ and $\mathbf{v}$, as

$$\mathbf{p} = [p(1), p(2), \ldots, p(N)]^T, \quad \mathbf{v} = [v(1), v(2), \ldots, v(N)]^T. \tag{6.1}$$

The BM, however, is assumed only to extend from element 2 to element N-1. Element 1 accounts for the stapes velocity, u_s in Fig. 8, whilst that the final element, N, accounts for the behaviour of the helicotrema. If the stapes velocity is set to zero, the vector of pressures due to the vector of BM velocities can be written as

$$\mathbf{p} = \mathbf{Z}_{FC}\mathbf{v}, \tag{6.2}$$

where $\mathbf{Z}_{FC}$ is the matrix due to fluid coupling. This matrix can be associated with two components, the one which accounts for the 1D propagation of the fluid and the near field component, which is associated with the 3D propagation of the fluid near the point of excitation, so that $\mathbf{Z}_{FC} = \mathbf{Z}_F + \mathbf{Z}_N$. In the same way, the vector of BM velocities can be

written as

$$\mathbf{v} = -\mathbf{Y}_{BM}\mathbf{p}, \tag{6.3}$$

where $\mathbf{Y}_{BM}$ is the diagonal mobility matrix, as it is assumed to react only locally. The diagonal elements represent the admittance of each micromechanical element at a given frequency, and extend only from 2 to $N-1$. It is formed as

$$\mathbf{Y}_{BM} = j\frac{\omega\rho}{H}\begin{bmatrix} 0 & & & & \\ & Y_{cp}(2) & & & \\ & & \ddots & & \\ & & & Y_{cp}(N-1) & \\ & & & & 0 \end{bmatrix}, \tag{6.4}$$

The total vector of velocities from cam be obtained using linear superposition, so that

$$\mathbf{v} = \mathbf{v}_S - \mathbf{Y}_{BM}\mathbf{p}, \tag{6.5}$$

where $\mathbf{v}_S$ is defined as the sources vector, being its first element equal to the stapes velocity, and the rest to zero

$$\mathbf{v}_s = \begin{bmatrix} u_s t & 0 & \cdots & 0 \end{bmatrix}^T. \tag{6.6}$$

By combining Equations 6.2 and 6.5 two expressions that account for the coupled response of the fluid and BM dynamics are obtained.[3]

$$\mathbf{v} = \left[\mathbf{I} + \mathbf{Y}_{BM}\mathbf{Z}_{FC}\right]^{-1}\mathbf{v}_s, \tag{6.7}$$

$$\mathbf{p} = \left[\mathbf{Z}_{FC}^{-1} + \mathbf{Y}_{BM}\right]^{-1}\mathbf{v}_s, \tag{6.8}$$

6.2 1D Fluid Coupling

The far field component of the pressure difference or 1D fluid coupling, can be obtained by using a wavenumber analysis[18, 7]. Alternatively, the pressure distribution can be obtained analytically from the solution of the differential equation for the far field coupling[7], as

$$p_l(n) = \frac{j16\omega\rho\Delta^2 v_0}{\pi^2}\sqrt{B(n_0)B(n)}\sum_{n'=n_0}^{N}\frac{1}{S_F(n')}, \quad 0 < n < n_0 - 1, \tag{6.9}$$

$$p_l(n) = \frac{j16\omega\rho\Delta^2 v_0}{\pi^2}\sqrt{B(n_0)B(n)}\sum_{n'=n}^{N}\frac{1}{S_F(n')}, \quad n_0 < n < N, \tag{6.10}$$

where $S_F(x)$ is the effective chamber area, given by

$$S_F(x) = \frac{S_1(x)S_2(x)}{S_1(x) + S_2(x)}, \tag{6.11}$$

being $S_1(x)$ and $S_1(x)$ are the upper (scala media and scala vestibuli) and lower (scala tympani) chambers, that for the case of this model reduces to be WH as this quantities are constant along the cochlea (symmetric scalaes), and $n' = |n - n_o|$, where n_0 is the element being excited. For a one dimensional propagation of the fluid, the columns of $\mathbf{Z}_{FC}$ can be

[3] A complete description can be found here[17].

obtained by normalizing Eqs. 6.9 and Eq. 6.10 by the input velocity, v_0.

6.3 3D fluid Coupling

The formulation of the pressure difference due to the fluid can be extended so that the effects of the near field, or 3D propagation, taking in account higher order fluid modes, are also considered. In this case, the pressure difference is due to far and near field components, so that

$$p_{FC} = p_L + p_N, \tag{6.12}$$

where the subscript L stands for long wave and the subscript N stands for near field. Consequently, the fluid coupling matrix is now formed

$$\mathbf{Z}_{FC} = \mathbf{Z}_L + \mathbf{Z}_N, \tag{6.13}$$

where $\mathbf{Z}_L$ is given by normalizing by the input velocity Equations 6.9 and 6.10.

The effective thickness th of the BM due to fluid loading can be calculated using[7]

$$T = \frac{8BH}{3\pi^3 W} + \sum_{n=1}^{\infty} \coth(n\pi H/W) \left[\frac{\cos(n\pi C/W) + \cos(n\pi(C+B)/W)}{1 - n^2 b^2/W^2} \right]^2, \tag{6.14}$$

where B is the width of the basilar membrane and W and H are the physical width and height of one cochlear chamber. At a given point along the cochlea, the near field pressure is given by

$$p_N = j\omega_0 \rho_0 T v_0. \tag{6.15}$$

The near field pressure distribution along the cochlea is obtained using an approximation to the averaged near field pressure due to a single element of the BM, obtained from [7], so that

$$p_N(n) = j\omega_0 \rho_0 \left(Q_1 e^{-n'\Delta/l_1} + Q_2 e^{-n'\Delta/l_2} \right) v_0, \tag{6.16}$$

where $Q_1 =$ and Q_2 are a function of T and l_1 equal to W/4.85 and l_2 to W/17.92[4]. The columns of the 3D fluid coupling matrix, $\mathbf{Z}_N$, are obtained by normalizing both the far field and the near field pressures at each position by the input velocity.

6.4 Comparative of fluid coupling configurations

Three different fluid coupling configurations can be used to calculate the coupled response of the cochlea. This depend on the magnitude of the higher order modes used to account for the 3D propagation. These configurations are:

1D fluid coupling

In this case the pressure due to the 1D propagation of the fluid is obtained from Equations 6.9 and 6.10. At the position of excitation, a delta symbolises the added mass due to the loading of the 3D propagation of the fluid, as can be observed in Fig. 10a, so that

$$p_N(x) = M_{FC}\delta(x - x_0). \tag{6.17}$$

[3]This approximation is used here for convenience, but the same result can be obtained by inverse Fourier transformation of the wavenumber of the fluid coupling[7].

[4]Values adapted from[7] for a 25 mm cochlea.

The mass of the BM is obtained by the original value given by Ramamoorthy *et al.*[1], plus the value due to the effective thickness of the BM, which symbolises the delta function $\delta(x - x_0)$.This allows the total "effective" mass of the BM, including near field fluid loading, to be taken in account, allowing the mechanics of the organ of Corti to be studied. The pressure distribution at an excitation point can be observed in Fig. 10a, and the coupled response obtained with this fluid distribution is shown in Fig. 11.

3D fluid coupling

In this case the 3D fluid propagation is given by Eq. 6.14, using the dimensions of the BM and cochlear box as given by Ramamoorthy *et al.*[1]. The fluid coupling matrix is formed as in Eq. 6.13. The BM mass has the value given in Ramamoorthy *et al.*[1],which is, m_{BM}=0.007$_{\text{(base) to}}$ 0.001 $_{\text{(apex)}}$ kg m^{-2}, and the extra mass due to the fluid near field is implicit included in the fluid coupling. The pressure distribution at an excitation point using this configuration is shown in Fig. 10b, and the results for the velocity distribution of the coupled cochlea in Fig. 12.

Diminished 3D coupling with extra mass

This configuration is a combination of the 1D and 3D cases. In this case the fluid coupling matrix is formed as

$$\mathbf{Z}_{FC} = \mathbf{Z}_L + 0.2\mathbf{Z}_N, \tag{6.18}$$

where $\mathbf{Z}_N$ has been obtained from Eq. 6.14 with the cochlear box and BM dimensions given by Ramamoorhty *et al.*[1]. The BM mass is obtained using the original BM mass value given combined with a reduced effective thickness of the BM due to fluid loading

$$m_{BM} = 0.007 - (0.007 - 0.001)\frac{x}{L} + 0.87\rho_f T. \tag{6.19}$$

The magnitude of the near field pressure is also reduced to a 20% of its expected value. In the same way the added mass due to the effective width of the BM is also reduced, to give room to the extra mass due to 20% of higher order fluid modes. This combination has been determined heuristically, and is chosen because it is believed that the fluid coupling description used by Ramamoorhty *et al.*[1] is much smaller than that which is obtained with Eq.6.14. This is due to the fact that Ramamoorthy *et al.*[1] use a FE model, and it has been found that in this kind of models the extent of the near field fluid coupling loading is very dependant on the number of fluid elements used[13]. The pressure distributions due to the fluid coupling that can be obtained using this configuration are shown, for some points along the cochlea, in Fig. 9.

The pressure distribution of this fluid coupling configuration is similar to that of the 1D case, in where a delta function of pressure loading at the excitation position simulates the added BM. However, as the delta is combined with the reduced amount of higher order modes, its base is broadened, as it can be observed in Fig. 10c. This fluid coupling configuration leads to the coupled results shown in Fig. 13, which is most like the results of Ramamoorhty *et al.*[1].

Interestingly, results that bear a reasonable resemblance to those with a diminished 3D fluid coupling component, but with a fluid chamber area that is uniform along the

length of the cochlea, can be obtained by assuming a full 3D fluid coupling but with a more realistic distribution of fluid chamber area along the cochlea, as discussed in Appendix A.

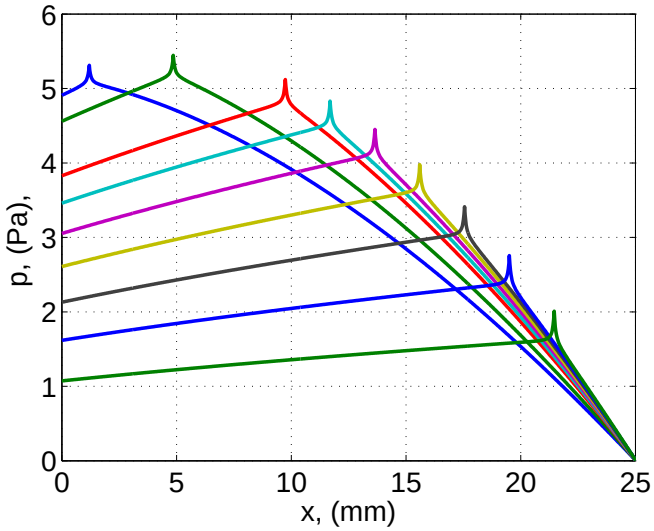

Figure 9: Distribution of the pressure difference using a diminished 3D fluid coupling model, in which variation of the BM width is taken in account. Response at x= 1.2 mm, 4.9 mm, 11.7 mm 13.6 mm, 15.6 mm, 17.6 mm 19.5 mm and 21.5 mm, with a velocity of 10 mm s^{-1} at a frequency of 1 kHz.

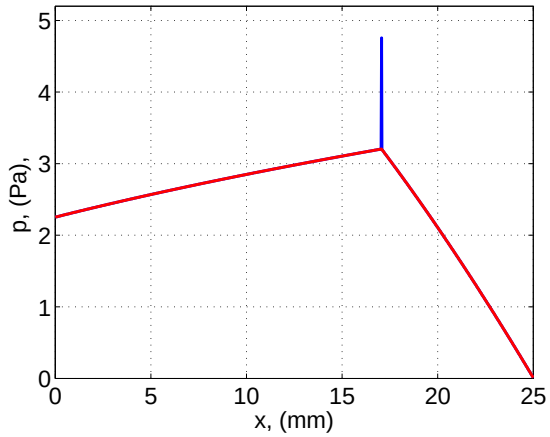

(a) 1D fluid coupling

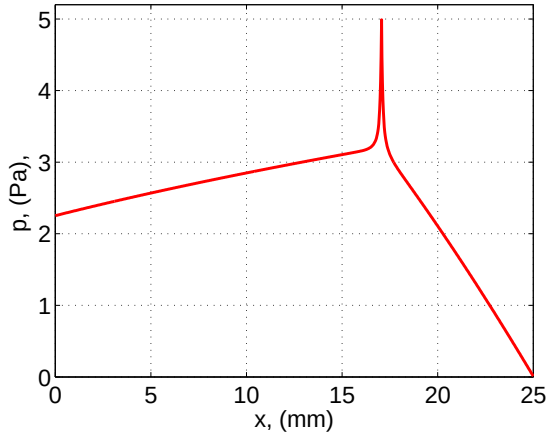

(b) 3D fluid coupling

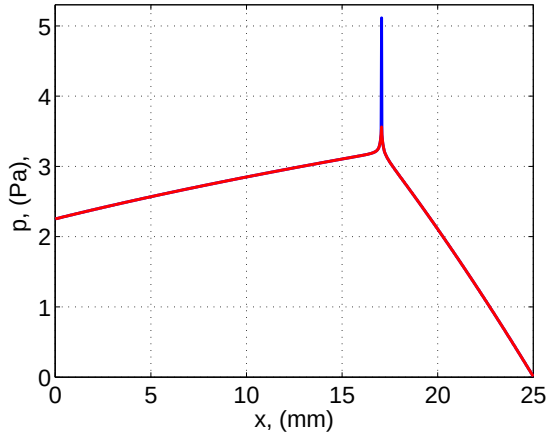

(c) Diminished 3D fluid coupling

Figure 10: Total pressure distributions, including increased effective BM thickness, for the different fluid coupling configurations, with a BM excitation at 17 mm. The delta function components in blue deltas symbolise the added mass due to the effective thickness of the BM, whilst that the delta function components in red component are due to fluid coupling.

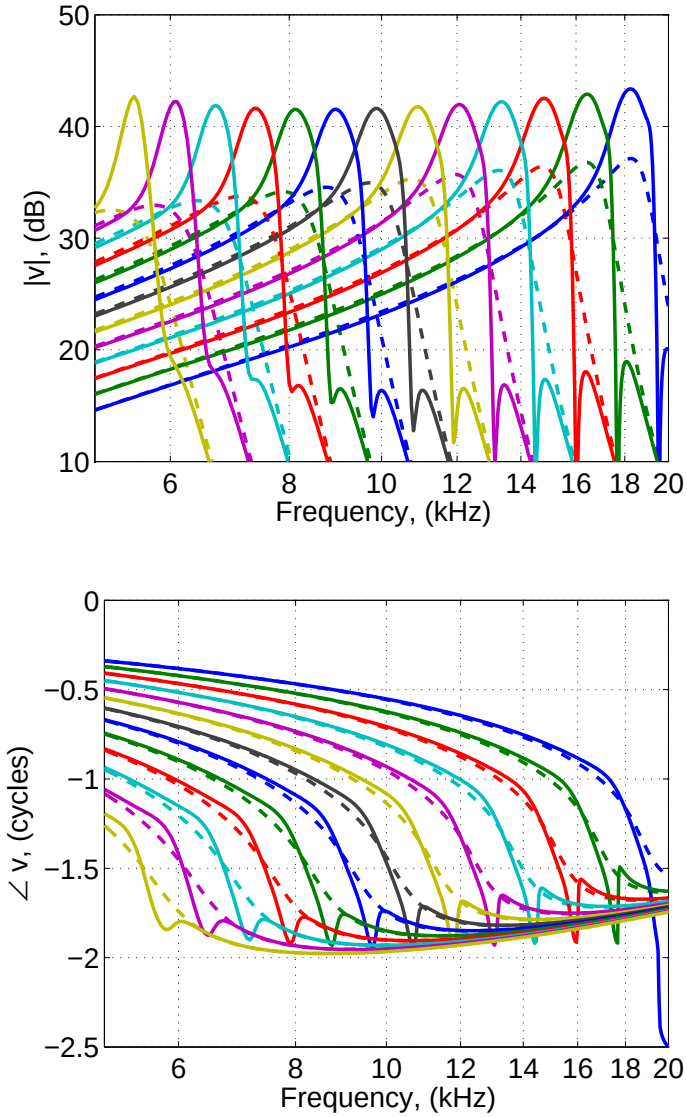

Figure 11: Response of the whole coupled active and passive cochlea using 1D fluid coupling. Response at x= 10.7 mm, 10.2 mm, 9.7 mm, 9.3 mm, 8.8 mm, 8.3 mm, 7.8 mm, 6.8 mm, 6.3 mm, 5.8 mm, 5.3 mm and 4.9 mm.

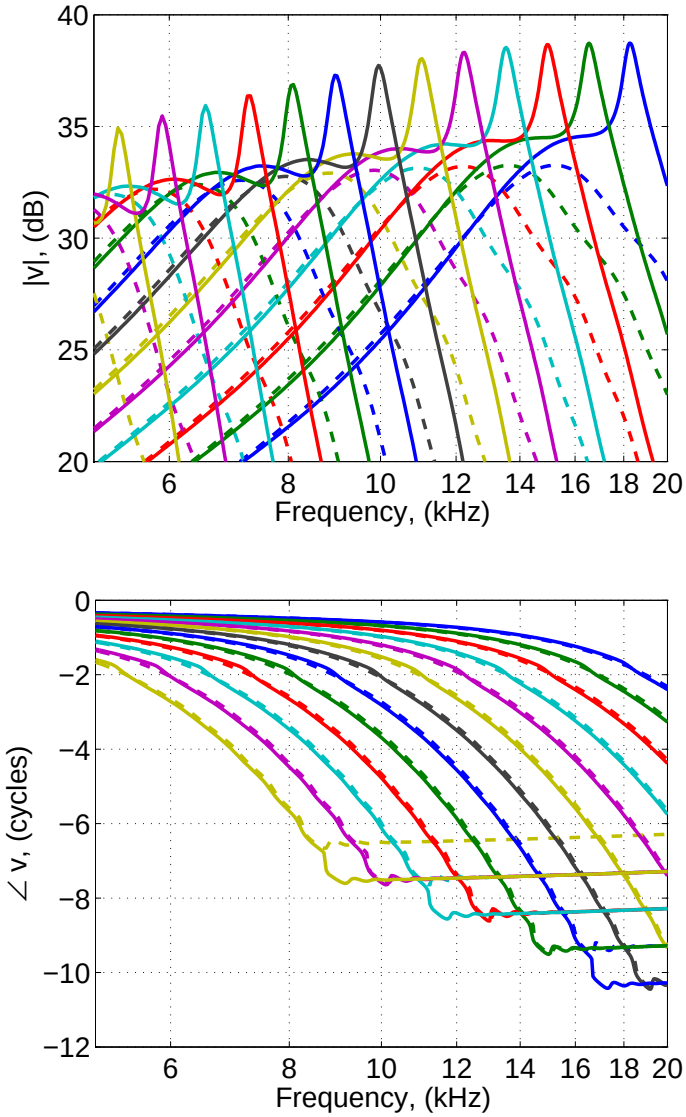

Figure 12: Response of the whole coupled active and passive cochlea using full 3D fluid coupling. Response at x= 10.7 mm, 10.2 mm, 9.7 mm, 9.3 mm, 8.8 mm, 8.3 mm, 7.8 mm, 6.8 mm, 6.3 mm, 5.8 mm, 5.3 mm and 4.9 mm.

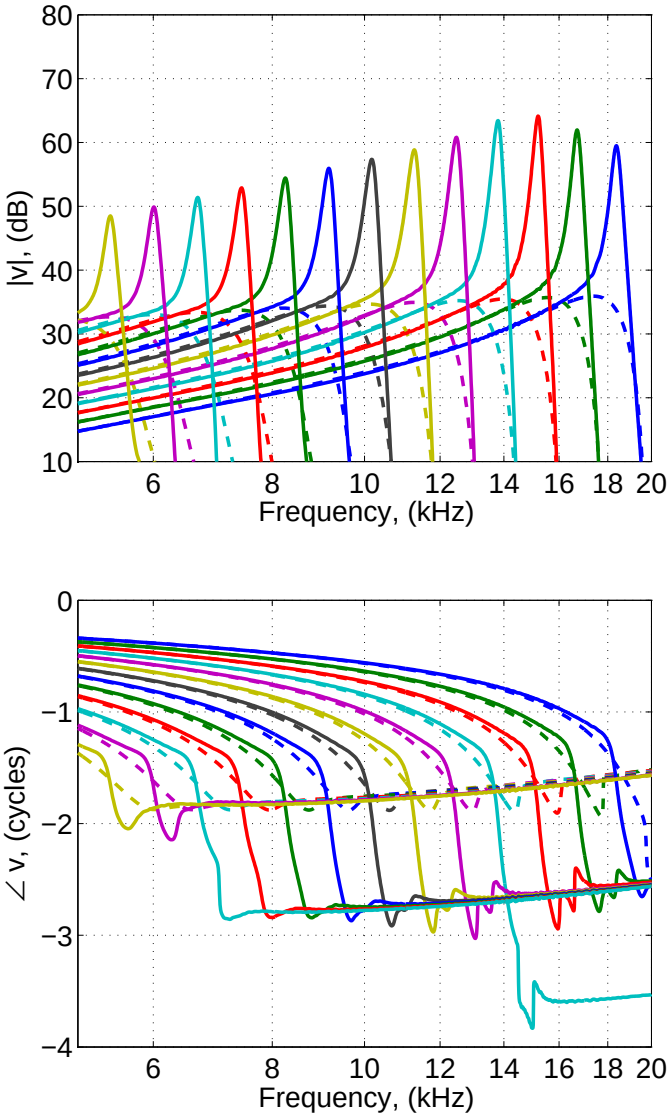

Figure 13: Response of the whole coupled active and passive cochlea using diminished 3D fluid coupling. Response at x= 10.7 mm, 10.2 mm, 9.7 mm, 9.3 mm, 8.8 mm, 8.3 mm, 7.8 mm, 6.8 mm, 6.3 mm, 5.8 mm, 5.3 mm and 4.9 mm.

7 The dynamics of the organ of Corti at some positions in the cochlea

7.1 Introduction

In this section we first discuss the dynamic response of the individual quantities defined in Section 3, these are: The receptance of the BM when this is excited by the acoustic pressure, G_{BA}, Eq. 3.8; the receptance of the BM when excited by the force due to the OHC electromotility, G_{BO}, Eq. 3.9; the displacement of the stereocillia of the OHC, when excited by the acoustic pressure that drives the BM, G_{SA}, Eq. 3.12; and when the stereocillia is displaced by the contraction of the OHC, G_{SO}, Eq. 3.15. These values are calculated at different positions along the cochlea: 5.75 mm, 8.75 mm and 11.75 mm, in order to reproduce the results presented by Ramamoorthy *et al.*[1].

Also presented, for the same positions along the length of the cochlea, are the exact parameters of the micromechanical model, together with the natural frequencies and vibration modes. The Bode and Nyquist diagrams for the closed-loop response, HG_{SO}, are also shown. These are shown considering H unity and considering H as defined in the Appendix C, in order to create a feedback loop as the one described in Section 5.

Finally the frequency response of the cochlea is plotted, together with the impulse response (IR) at each correspondent position for active and passive cases, for the coupled model with a fluid configuration which uses diminished 3D fluid propagation, together with an added mass. There are also plotted the frequency glides which correspond for a fully active case, together with Bode plots of the micromechanical element which corresponds to the position of study, for both responses, fully active and fully passive.

7.2 5.75 mm

Fig. 14 shows the individual frequency responses due to the excitation of individual modes, whose natural frequency and mode shapes are listed in Table. 3 at this position. The responses between the fluid pressure excitation and the BM response, G_{BA}, clearly shows the BM mode at around 15 kHz, and thus for the OHC excitation to the stereocillia response, G_{SO}, has a peak at above 16.4 kHz, corresponding to the TM mode. Also shown, for reference, are the individual responses of the RL and TM, w_{RL} and w_{TM}, when excited by the OHC, where G_{SO} is the difference between these responses.

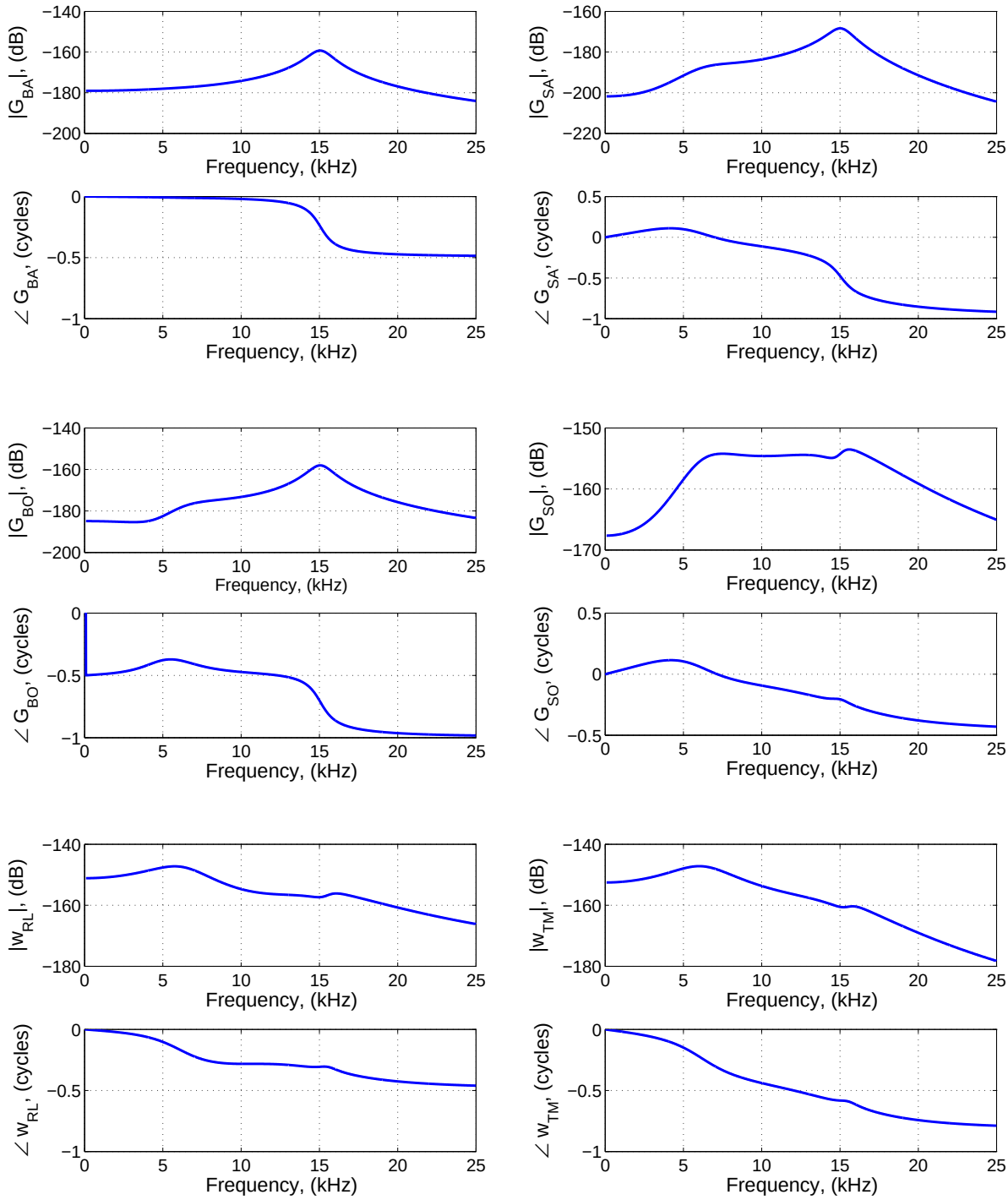

Figure 14: Dynamics of the micromechanical model at 5.75 mm normalized to 1m·Pa^{-1}. w_{RL} and w_{TM} represent the case when these are excited by p_{OHC}.

Table 2: Value for the parameters of the micromechanical model at 5.75 mm.

Element	Value	Units
k_1	$8.89145{\cdot}10^8$	Nm^{-3}
k_2	$1.7439{\cdot}10^7$	Nm^{-3}
k_3	$4.9049{\cdot}10^7$	Nm^{-3}
k_4	$1.5738{\cdot}10^7$	Nm^{-3}
k_5	$1.0900{\cdot}10^7$	Nm^{-3}
m_1	0.1043	kgm^{-2}
m_2	0.0110	kgm^{-2}
m_3	0.0110	kgm^{-2}
c_1	$0.9293{\cdot}10^3$	Nsm^{-3}
c_2	$0.0000{\cdot}10^3$	Nsm^{-3}
c_3	$0.2230{\cdot}10^3$	Nsm^{-3}
c_4	$0.4646{\cdot}10^3$	Nsm^{-3}
c_5	$0.0000{\cdot}10^3$	Nsm^{-3}

Table 3: Natural frequencies and vibration modes of the micromechanical model at 5.75 mm.

	BM mode	TM mode	RL mode
Natural frequency, (kHz)	15.0	16.4	6.3
Normalised displacement of m_1	-3.05	-0.73	0.14
Normalised displacement of m_2	-1.45	7.18	6.00
Normalised displacement of m_3	-1.22	-5.77	7.31

The response of the feedback path, H, in Fig. 7, reproduces the action of the OHC, from stereocillia deflection to OHC pressure. A simplified model of the OHC is discussed in Appendix C, which suggests that the frequency response of H can be reasonably approximated by

$$H(j\omega) = \frac{\gamma g_H}{1 + \frac{j\omega}{\omega_{OHC}}}, \tag{7.1}$$

where γ is a nondimensional OHC gain between 0 and 1, g_H is an overall response given by Eq. C.7 and ω_{OHC} is the cutoff frequency, given by the reciprocal of its electrical resistance multiplied by its electrical capacitance. The cut-off frequency of the OHC, $\omega_{OHC}/2\pi$, is about 270 Hz from the parameters at x=5.75 mm, and so is much less than the natural frequency of the BM and the TM.

Fig. 15 shows the frequency response of the open loop response in Fig. 7, equal to HG_{SO}. The low pass characteristic and additional 0.5 cycles of phase lag from H are clear with the frequency response of G_{SO} in Fig. 14. Also shown are the Nyquist plot of HG_{SO}, showing that with the adequate gain in H it comes close to the Nyquist point at about 16.4 kHz, and the resulting closed-loop frequency response.

Fig. 16 shows the BM velocity due to the coupled response of the cochlea with $\gamma = 0$, passive, and $\gamma = 1$, active, together with its impulse response and frequency glide. In the same figure there is also shown the frequency response of the micromechanical element at 5.75 mm from the base, for active and passive cases. The value of the mobility is slightly decreased for frequencies lower than that of the CF, and observes a big reduction

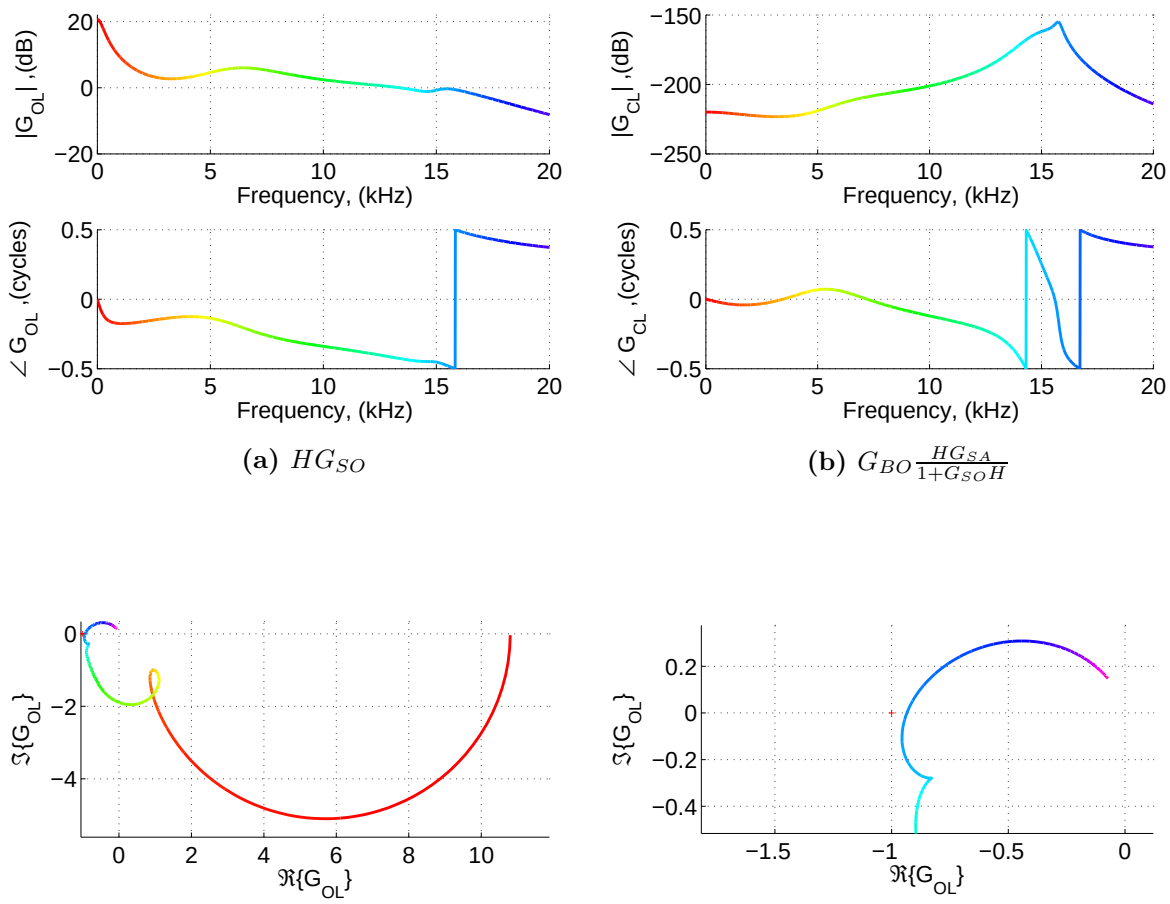

(a) HG_{SO} **(b)** $G_{BO}\frac{HG_{SA}}{1+G_{SO}H}$

(c) HG_{SO} **(d)** Details of HG_{SO}

Figure 15: The upper plots show the Bode plots of the open loop response, $G_{OL} = HG_{SO}$, and the closed loop response, $G_{CL} = G_{BO}\frac{HG_{SA}}{1+G_{SO}H}$. The lower plots show the Nyquist diagram of G_{OL}, and a zoom where it is close to (-1,0). All the responses correspond to the micromechanical element of 5.75 mm.

for frequencies just above the CF. This contrasts with the results shown by [19] for the Neely and Kim 1986 model, where the value of the active mobility remained high after the CF. Similar results are observed for the mobility of the BM, and how this varies along the length of the cochlea when is excited by a single frequency. The value of the mobility is slightly decreased in positions basal to the resonance and greatly increased just at the resonance. After the resonance, it experiments a large reduction.It is also shown the frequency response of the mobility of the BM, and how this varies along the length of the cochlea when is excited by a single frequency. As previously observed by Ku[19], the value of the mobility is slightly decreased in positions basal to the resonance and greatly increased after the resonance, so that the motion of the BM is decreased at positions apical to the CF. It is strange that the phase of Y_{BM} seems to be between ± 0.25 cycles at all position, so its peak part is positive, even when it is active.

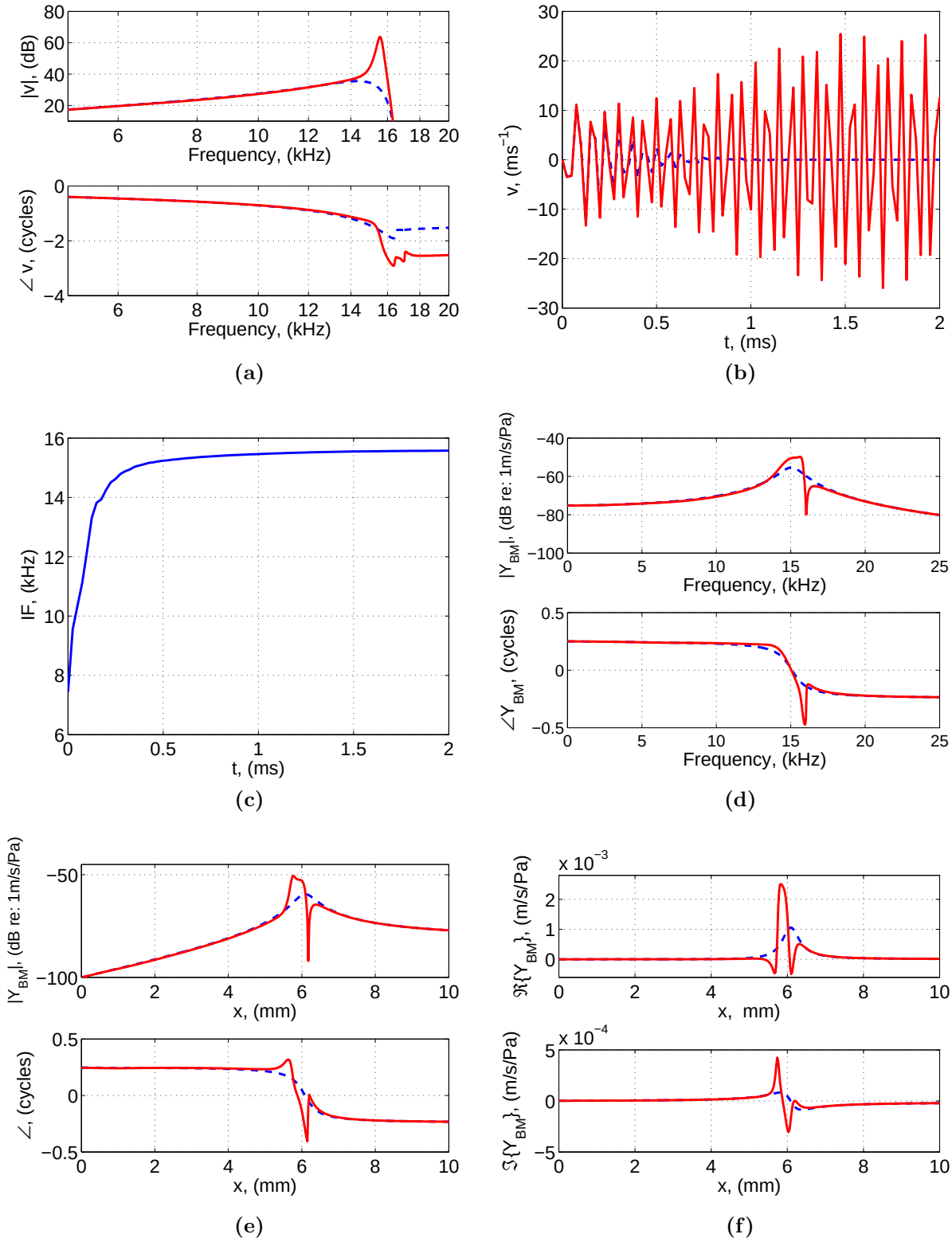

Figure 16: Coupled response normalised to the stape's velocity, (a), impulse response, (b), and frequency glide of the BM's velocity, (c), being the responses estimated at 5.75 mm from the base. Graph (d) shows the frequency response of the mobility of the micromechanical element at 5.75 mm, and graphs (e) and (f) show the mobility of the isolated BM dynamics along its length when excited by the CF of 5.75 mm.

7.3 8.75 mm

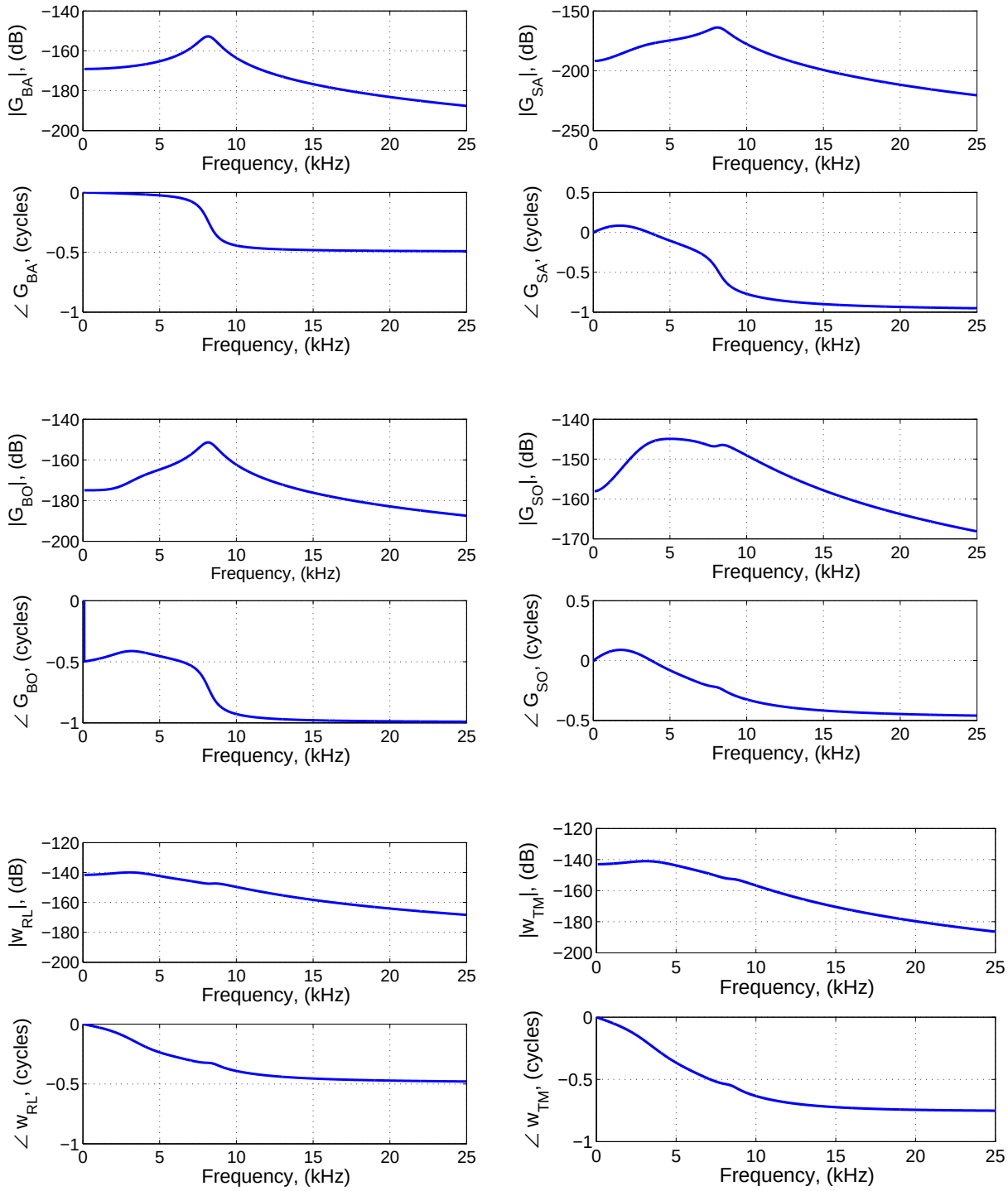

Figure 17: Dynamics of the micromechanical model at 8.75 mm normalized to $1\text{m}\cdot\text{Pa}^{-1}$. w_{RL} and w_{TM} represent the case when these are excited by p_{OHC}.

Table 4: Value for the parameters of the micromechanical model at 8.75 mm.

Element	Value	Units
k_1	$2.8276{\cdot}10^8$	Nm^{-3}
k_2	$5.8016{\cdot}10^6$	Nm^{-3}
k_3	$1.6317{\cdot}10^7$	Nm^{-3}
k_4	$7.1742{\cdot}10^6$	Nm^{-3}
k_5	$3.6260{\cdot}10^6$	Nm^{-3}
m_1	0.1092	kgm^{-2}
m_2	0.0113	kgm^{-2}
m_3	0.0113	kgm^{-2}
c_1	$0.8196{\cdot}10^3$	Nsm^{-3}
c_2	$0.0000{\cdot}10^3$	Nsm^{-3}
c_3	$0.1967{\cdot}10^3$	Nsm^{-3}
c_4	$0.4098{\cdot}10^3$	Nsm^{-3}
c_5	$0.0000{\cdot}10^3$	Nsm^{-3}

Table 5: Natural frequencies and vibration modes of the micromechanical model at 8.75 mm.

	BM mode	TM mode	RL mode
Natural frequency, (kHz)	8.2	9.3	3.6
Normalised displacement of m_1	-2.99	-0.48	0.14
Normalised displacement of m_2	-0.86	7.18	5.93
Normalised displacement of m_3	1.29	-5.81	7.22

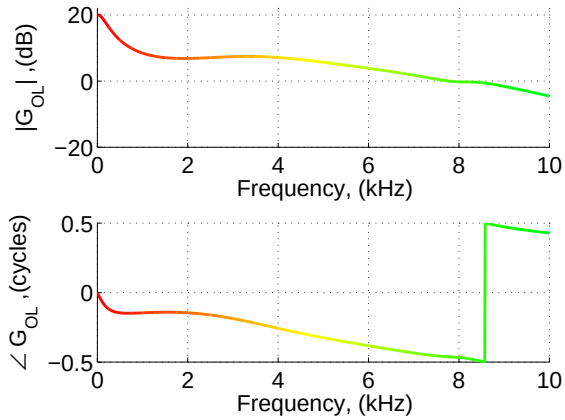

(a) HG_{SO}

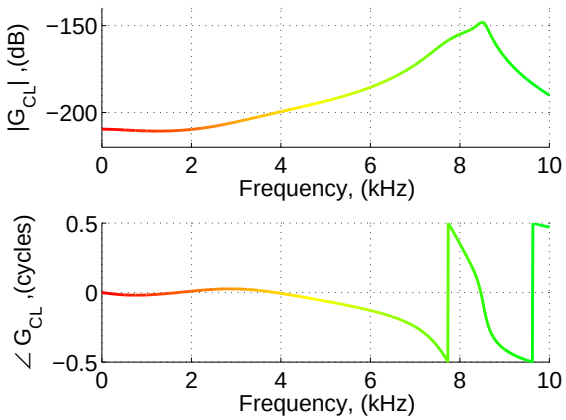

(b) $G_{BO}\frac{HG_{SA}}{1+G_{SO}H}$

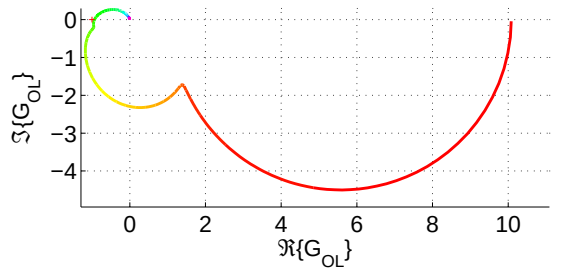

(c) HG_{SO}

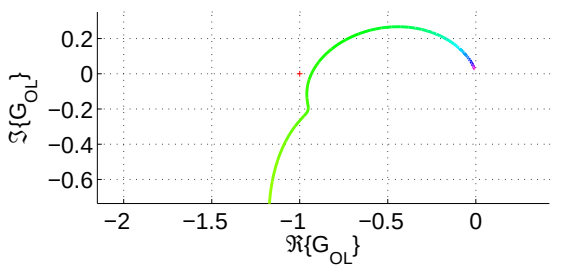

(d) Details of HG_{SO}

Figure 18: The upper plot show the Bode and diagrams of and HG_{SO} and the closed loop response, $G_{BO}\frac{HG_{SA}}{1+G_{SO}H}$. The lower plots show the Nyquist diagram of HG_{SO}, and a zoom where it is close to (-1,0). All the responses correspond to the micromechanical element of 8.75 mm.

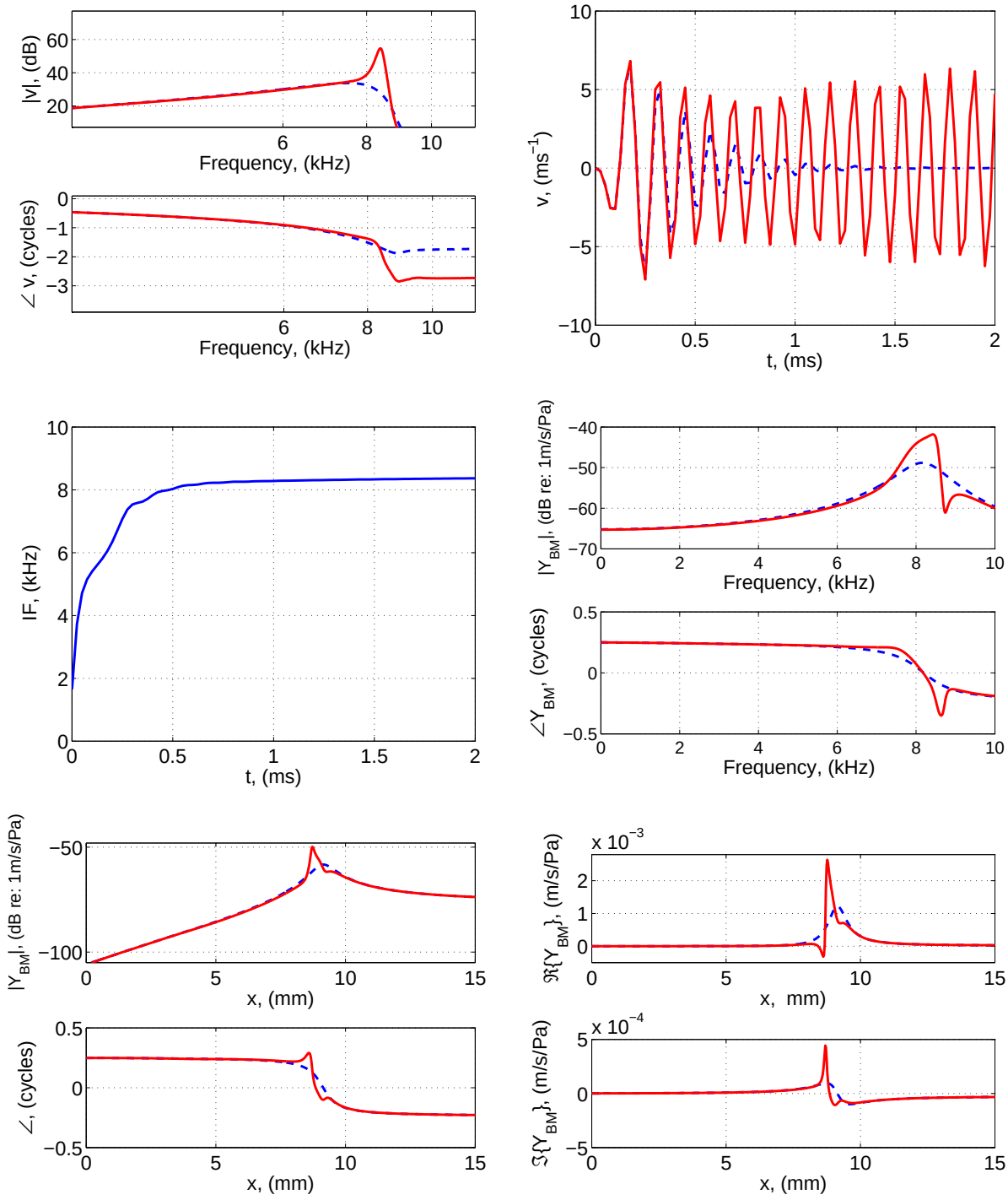

Figure 19: Coupled response normalised to the stape's velocity, (a), impulse response, (b), and frequency glide of the BM's velocity, (c), being the responses estimated at 8.75 mm from the base. Graph (d) shows the frequency response of the mobility of the micromechanical element at 8.75 mm, and graphs (e) and (f) show the mobility of the isolated BM dynamics along its length when excited by the CF of 8.75 mm.

7.4 11.75 mm

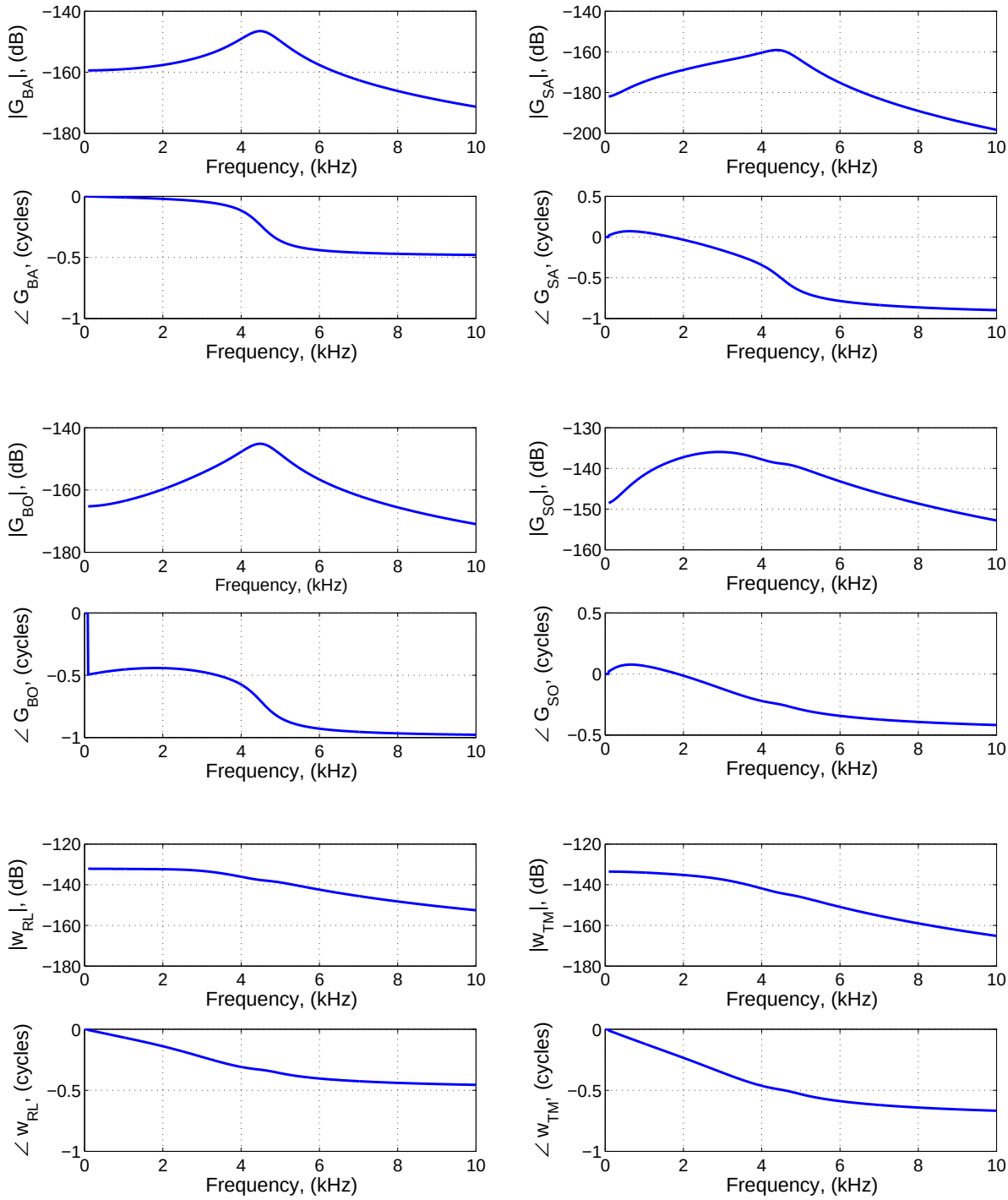

Figure 20: Dynamics of the micromechanical model at 11.75 mm normalized to 1m·Pa^{-1}. w_{RL} and w_{TM} represent the case when these are excited by p_{OHC}.

Table 6: Value for the parameters of the micromechanical model at 11.75 mm.

Element	Value	Units
k_1	$9.2575{\cdot}10^7$	Nm^{-3}
k_2	$1.9573{\cdot}10^6$	Nm^{-3}
k_3	$5.5049{\cdot}10^6$	Nm^{-3}
k_4	$3.3165{\cdot}10^6$	Nm^{-3}
k_5	$1.2233{\cdot}10^6$	Nm^{-3}
m_1	0.1166	kgm^{-2}
m_2	0.0117	kgm^{-2}
m_3	0.0117	kgm^{-2}
c_1	$0.7331{\cdot}10^3$	Nsm^{-3}
c_2	$0.0000{\cdot}10^3$	Nsm^{-3}
c_3	$0.1760{\cdot}10^3$	Nsm^{-3}
c_4	$0.3665{\cdot}10^3$	Nsm^{-3}
c_5	$0.0000{\cdot}10^3$	Nsm^{-3}

Table 7: Natural frequencies and vibration modes of the micromechanical model at 11.75 mm.

	BM mode	TM mode	RL mode
Natural frequency, (kHz)	4.5	5.3	2.0
Normalised displacement of m_1	-2.89	-0.38	0.15
Normalised displacement of m_2	-0.64	7.07	5.82
Normalised displacement of m_3	1.13	-5.73	7.08

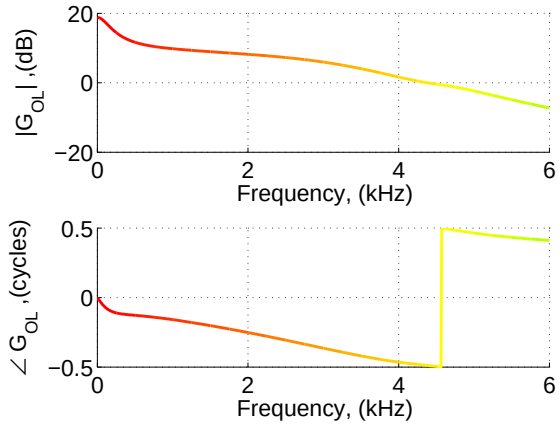

(a) HG_{SO}

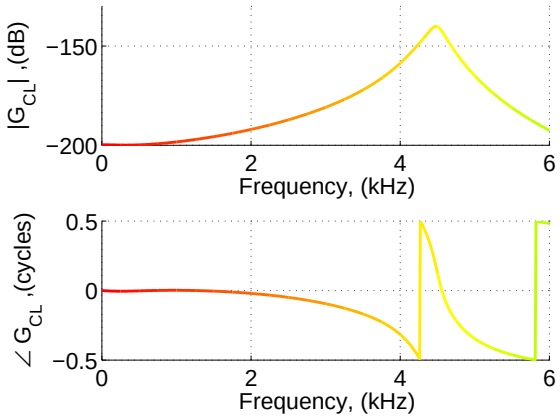

(b) $G_{BO}\frac{HG_{SA}}{1+G_{SO}H}$

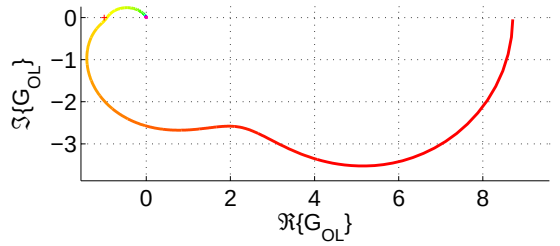

(c) HG_{SO}

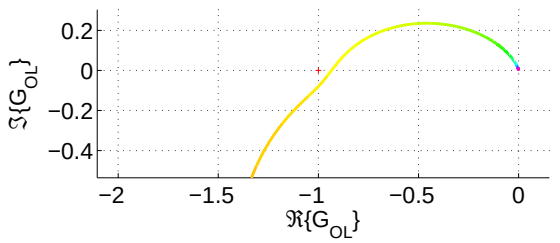

(d) Details of HG_{SO}

Figure 21: The upper plot show the Bode and diagrams of and HG_{SO} and the closed loop response, $G_{BO}\frac{HG_{SA}}{1+G_{SO}H}$. The lower plots show the Nyquist diagram of HG_{SO}, and a zoom where it is close to (-1,0). All the responses correspond to the micromechanical element of 11.75 mm.

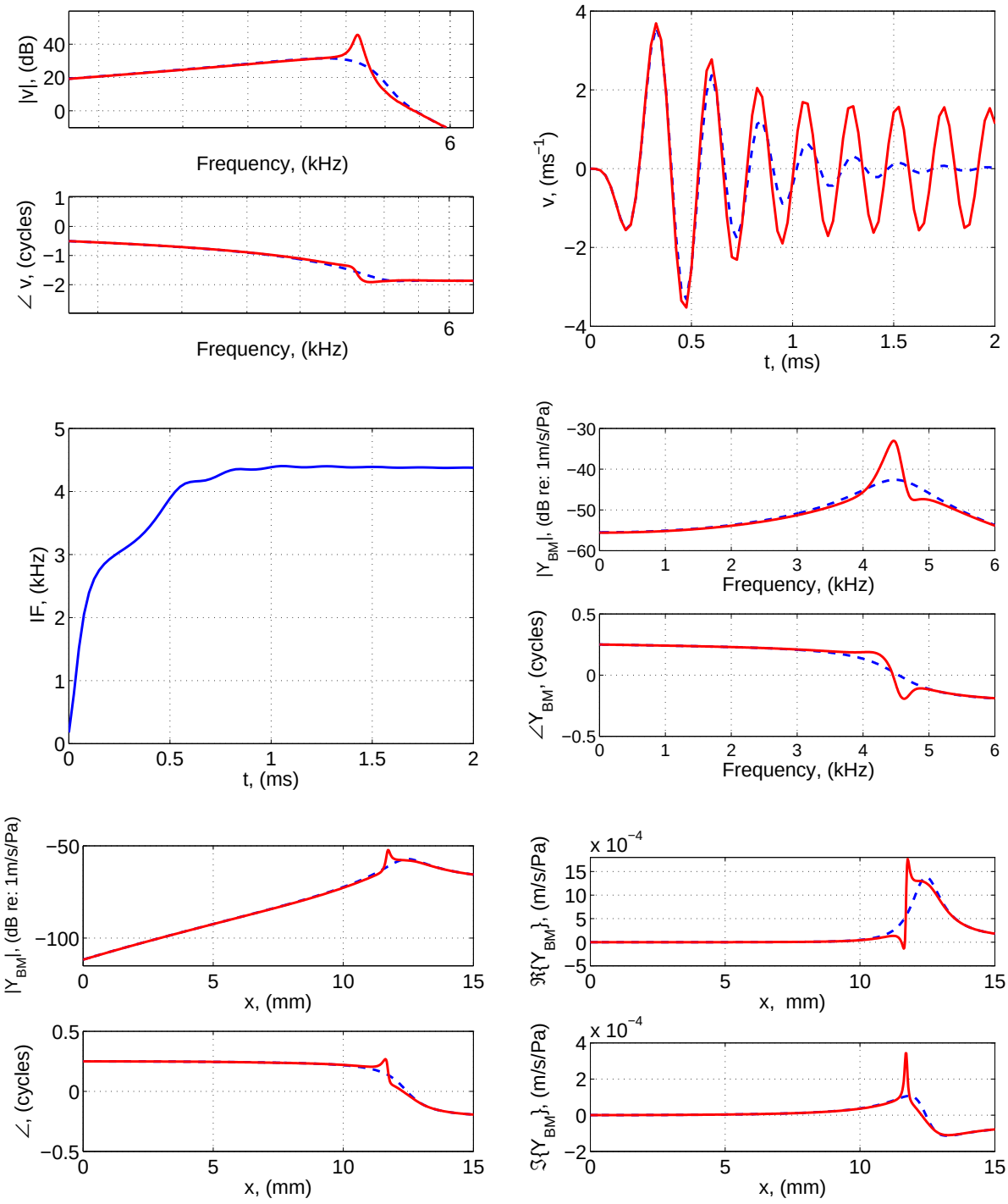

Figure 22: Coupled response normalised to the stape's velocity, (a), impulse response, (b), and frequency glide of the BM's velocity, (c), being the responses estimated at 11.75 mm from the base. Graph (d) shows the frequency response of the mobility of the micromechanical element at 11.75 mm, and graphs (e) and (f) show the mobility of the isolated BM dynamics along its length when excited by the CF of 11.75 mm.

8 Conclusions

A simplified version of the cochlear model of Ramamoorhty *et al.*[1] has been implemented. An elemental approach is used, with an analytic formulation for the fluid coupling and a lumped parameter model of the micromechanics.

The frequency response of the coupled response of the model, show a reasonable agreement with that of Ramamoorthy *et al.*[1]. The distribution of frequency with length in the BM is, however, slightly different from that of these authors, i.e., whilst for their results a point 11.75 mm away from the base presents a resonance at around 6.5 kHz, in the case of the results presented here this resonance is present at around 4 kHz. This shifting in frequency is thought to be caused by differences in the value of the total mass of the BM used.

It is also noted that the near field component of the fluid coupling impedance has had to be reduced in order to obtain similar results to Ramamoorhty *et al.*[1]. Careful reading of their paper suggests that the extent of their near field component, which is given by the number of radial modes accounted for, has been used by these authors as a tuning parameter to obtain realistic results.

The model presented here also includes a simplified piezoelectric model for the OHC, as justified in Appendix C, but also does not include longitudinal electrical coupling. This is shown in Fig. 15 of Ramamoorhty *et al.*[1] to significantly increase the stable active gain, and perhaps explains why the model described in this report has a maximum gain which is about 5 dB less than in [1].

With respect to the time response, the obtained velocity impulse responses predicted at different points in the cochlea show that the zero-crossings of the responses, are almost invariant of the active gain level used, especially for the first few cycles, in agreement with impulse response obtained from recorded measurements in a guinea-pig cochlea[20]. The plotted frequency glides also seem to be in qualitative agreement with those obtained from measurements in a guinea-pig cochlea[21], and are similar to that shown by the model of Ramamoorthy *et al.*[1].

References

[1] S. Ramamoorthy, N. V. Deo, and K. Grosh, "A mechano-electro-acoustical model for the cochlea: Response to acoustic stimuli," *The Journal of the Acoustical Society of America*, vol. 121, no. 5, pp. 2758–2773, 2007.

[2] J. B. Allen, "Cochlear micromechanics—a physical model of transduction," *The Journal of the Acoustical Society of America*, vol. 68, no. 6, pp. 1660–1670, 1980.

[3] S. J. Elliott, R. Pierzycki, and B.Lineton, "Lumped-parameter models for cochlear micromechanics," Institute of Sound and Vibration Research, University of Southampton, Tech. Rep., 2006.

[4] S. J. Elliott, "Active control of vibration in aircraft and inside the ear." Active 09 Conference (Ontario), 2009.

[5] S. J. Elliott and C. A. Shera, "The cochlea as a smart structure," *Smart Materials and Structures*, vol. 21, no. 6, p. 064001, 2012.

[6] C. Geisler and C. Sang, "A cochlear model using feed-forward outer-hair-cell forces," *Hearing Research*, vol. 86, no. 12, pp. 132 – 146, 1995.

[7] S. J. Elliott, B. Lineton, and G. Ni, "Fluid coupling in a discrete model of cochlear mechanics," *The Journal of the Acoustical Society of America*, vol. 130, no. 3, pp. 1441–1451, 2011.

[8] G. Zweig, R. Lipes, and J. R. Pierce, "The cochlear compromise," *The Journal of the Acoustical Society of America*, vol. 59, no. 4, pp. 975–982, 1976.

[9] C. A. Shera, A. Tubis, and C. L. Talmadge, "Coherent reflection in a two-dimensional cochlea: Short-wave versus long-wave scattering in the generation of reflection-source otoacoustic emissions," *The Journal of the Acoustical Society of America*, vol. 118, no. 1, pp. 287–313, 2005.

[10] S. T. Neely, "Mathematical modeling of cochlear mechanics," *The Journal of the Acoustical Society of America*, vol. 78, no. 1, pp. 345–352, 1985.

[11] O. de La Rochefoucauld and E. S. Olson, "The role of organ of corti mass in passive cochlear tuning," *Biophysical Journal*, vol. 93, no. 10, pp. 3434 – 3450, 2007.

[12] A. A. Parthasarathi, K. Grosh, and A. L. Nuttall, "Three-dimensional numerical modeling for global cochlear dynamics," *The Journal of the Acoustical Society of America*, vol. 107, no. 1, pp. 474–485, 2000.

[13] G. Ni, "Fluid coupling and waves in the cochlea," Ph.D. dissertation, Institute of Sound and Vibration Research, University of Southampton, November 2012.

[14] Y. Li, "Corrections regarding to JASA paper." 2012.

[15] D. D. Greenwood, "Comparing octaves, frequency ranges, and cochlear-map curvature across species," *Hearing Research*, vol. 94, no. 12, pp. 157 – 162, 1996.

[16] J. Tsuji and M. Liberman, "Intracellular labeling of auditory nerve fibers in guinea pig: central and peripheral projections," *The Journal of Comparative Neurology*, vol. 381, no. 2, pp. 188–202, 1997.

[17] S. J. Elliott, B. Lineton, and G. Ni, "ISVR Tehnical Memorandum 990, Fluid Coupling between the Elements in a Discrete Model of Cochlear Mechanics," Institute of Sound and Vibration Research, University of Southampton, Tech. Rep., 2010.

[18] C. R. Steele and L. A. Taber, "Comparison of WKB calculations and experimental results for three-dimensional cochlear models," *The Journal of the Acoustical Society of America*, vol. 65, no. 4, pp. 1007–1018, 1979.

[19] E. M. Ku, "Modelling the human cochlea," Ph.D. dissertation, ISVR, University of Southampton, 2008.

[20] E. de Boer and A. L. Nuttall, "The mechanical waveform of the basilar membrane. III. Intensity effects," *The Journal of the Acoustical Society of America*, vol. 107, no. 3, pp. 1497–1507, 2000.

[21] ——, "The mechanical waveform of the basilar membrane. i. frequency modulations ("glides") in impulse responses and cross-correlation functions," *The Journal of the Acoustical Society of America*, vol. 101, no. 6, pp. 3583–3592, 1997.

[22] C. Fernández, "Dimensions of the cochlea (guinea pig)," *The Journal of the Acoustical Society of America*, vol. 24, no. 5, pp. 519–523, 1952.

[23] A. Salt, "Cochlear fluds research laboratory, guinea pig cochlear chambers dimensions," 03 2013. [Online]. Available: http://oto2.wustl.edu/cochlea/

[24] S. J. Elliott, E. M. Ku, and B. Lineton, "A state space model for cochlear mechanics," *The Journal of the Acoustical Society of America*, vol. 122, no. 5, pp. 2759–2771, 2007.

[25] S. Cantrel and S. J. Elliott, "A model of the three-dimensional active cochlea," Master's thesis, Institute of Sound and Vibration Research, University of Southampton, Southampton, UK, 2012.

[26] C. A. Shera, "Intensity-invariance of fine time structure in basilar-membrane click responses: Implications for cochlear mechanics," *The Journal of the Acoustical Society of America*, vol. 110, no. 1, pp. 332–348, 2001.

[27] A. Preumont, *Mechatronics: Dynamics of electromechanical and piezoelectric systems*, ser. Solid mechanics and its applications. Berlin: Springer, 2006.

[28] X. X. Dong, M. Ospeck, and K. H. Iwasa, "Piezoelectric Reciprocal Relationship of the Membrane Motor in the Cochlear Outer Hair Cell," *Biophysical Journal*, vol. 82, no. 3, pp. 1254–1259, 2002.

[29] K. Iwasa, "A two-state piezoeletric model for the outer hair cell motility," *Biophysical Journal*, vol. 81, pp. 2495–2506, 2001.

[30] N. V. Deo and K. Grosh, "Two-state model for outer hair cell stiffness and motility,," *Biophysical Journal*, vol. 82, pp. 1254–1259, 2004.

[31] D. O. Maoiléidigh and F. Jülicher, "The interplay between active hair bundle motility and electromotility in the cochlea," *The Journal of the Acoustical Society of America*, vol. 128, no. 3, pp. 1175–1190, 2010.

Appendices

A Response of the model using realistic cochlear chamber dimensions

This appendix presents the response of the model using different cochlear chamber dimensions, which are based on the real dimensions of the cochlear chambers of a guinea-pig. By the use of the parameters presented here it is possible to use a 3D fluid coupling configuration, such as the one described in Section 6.4.

The dimensions used have been these obtained by Fernández[22] and those by Salt[23], whose values are much smaller of that used by Ramamoorhty *et al.*[1]. Fig. 23 shows the areas of upper (scala media and scala vestibuli) and lower (scala tympani) cochlear chambers, as given by Salt[23]. These values, however, have been extended from 15 mm until 25 mm.

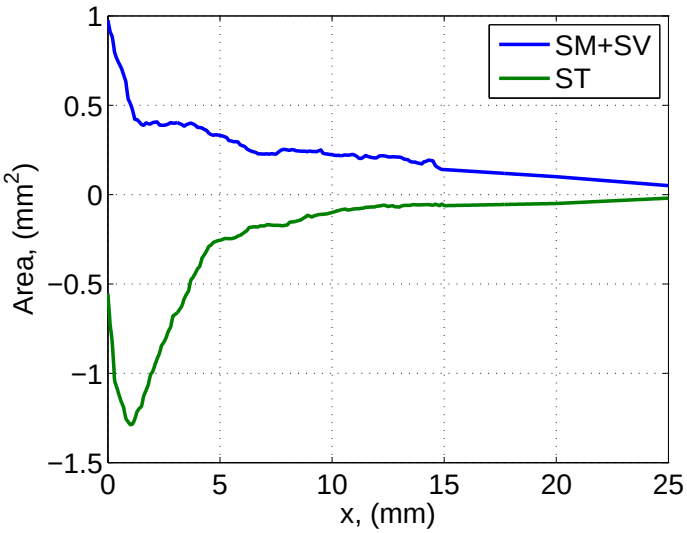

Figure 23: Variation in the upper and lower cochlear chamber areas, as assumed by Salt until 15 mm. From 15 mm to 25 mm the values have been assumed.

The width of the cochlear partition, W, has been estimated from that given by Fernández[22]. The height of the chambers, H, has been obtained from diving the effective area, S_F, as defined in Eq. 6.11, by the width of the cochlear partition. The width of the BM is that given by Ramamoorhty *et al.*[1]. The distribution of these parameters along the length of the cochlea can be observed in Fig. 24.

The pressure distribution along the basilar membrane is obtained using Eqs. 6.9 and 6.10 for calculating the far field pressure component, and Eqs. 6.14 and 6.16 for calculating the near field pressure component. The pressure distribution results using the dimensions here defined is shown in Fig. 25. For this configuration the value of the pressure due to the far field is much bigger than that if the parameters given by Ramamoorthy *et al.* are used (shown in Fig. 9). This is caused by the fact for the parameters used in this section, the BM width is more similar to that of the cochlear chambers, keeping a ratio b_{BM}/H much

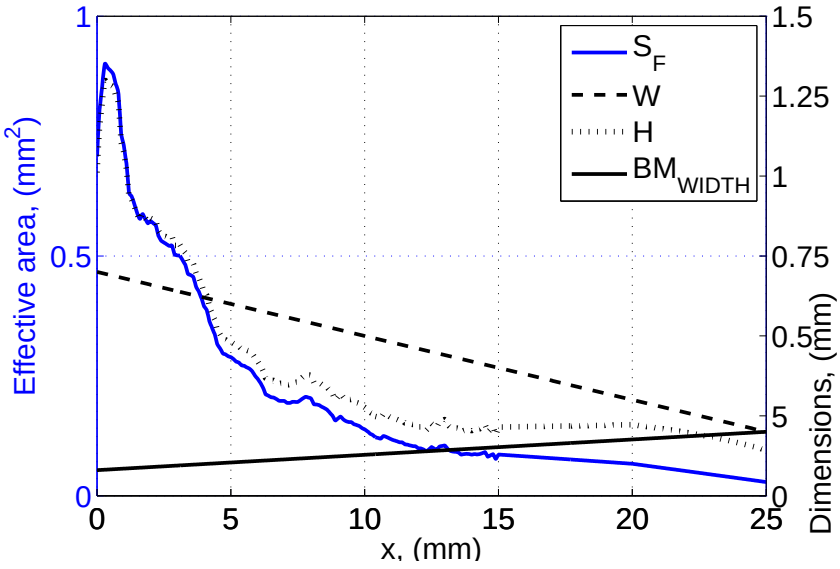

Figure 24: Calculated effective area for the pressure difference, S_F, (left y axis, blue graph). The right y axes graphs, plotted in black, show the effective height and width of the cochlear chambers, and the width of the BM.

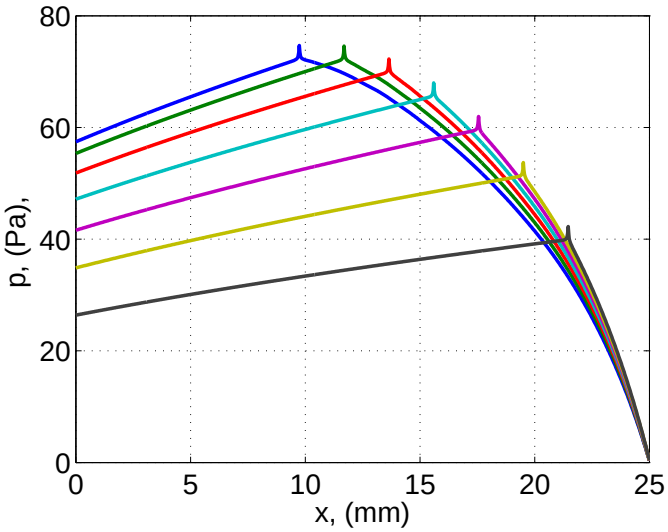

Figure 25: Distribution of the pressure difference using full 3D fluid coupling, in which the variation of the BM width and the change in fluid chamber area along the cochlea are taken in account. Response at x= 1.2 mm, 4.9 mm, 11.7 mm 13.6 mm, 15.6 mm, 17.6 mm 19.5 mm and 21.5 mm, with a velocity of 10 mm s^{-1} at a frequency of 1 kHz.

bigger than that used by Ramamoorhty *et al.*[1].

The coupled response is shown in Fig. 26, and in Fig. 27 using a 3D coupling configuration. The responses have been calculated using also different values for the dynamic elements from that for the results presented in the main document. The value used for k_{OHC} is three times the value given in Table 1. $m_{TM}(0)$ has been selected to be of 0.018 kg m^{-2} and m_{RL} to be $0.7m_{TM}$, as originally used by Ramamoorthy *et al.*[1].

May be that in the case of the model presented here, with three masses, it is needed

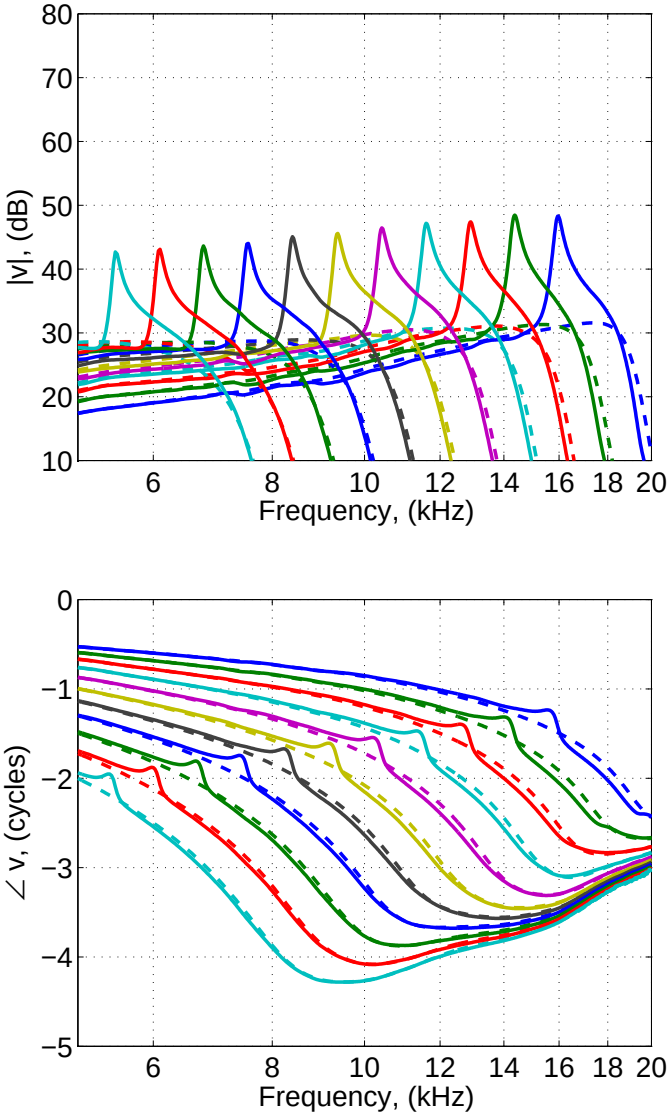

Figure 26: Response of the whole coupled active and passive cochlea using 1D fluid coupling with realistic cochlear chamber values. Response at x=10.2 mm, 9.7 mm, 9.3 mm, 8.8 mm, 8.3 mm, 7.8 mm, 6.8 mm, 6.3 mm, 5.8 mm and 5.3 mm.

to take in account the effect of the fluid loading in the mass of the TM, although, this is however, difficult to model. The results with 3D fluid coupling presented here show a frequency response slightly different from that presented by Ramamoorhty *et al*[1], but one which is not too far away from measurements in guinea-pig cochleas[20].

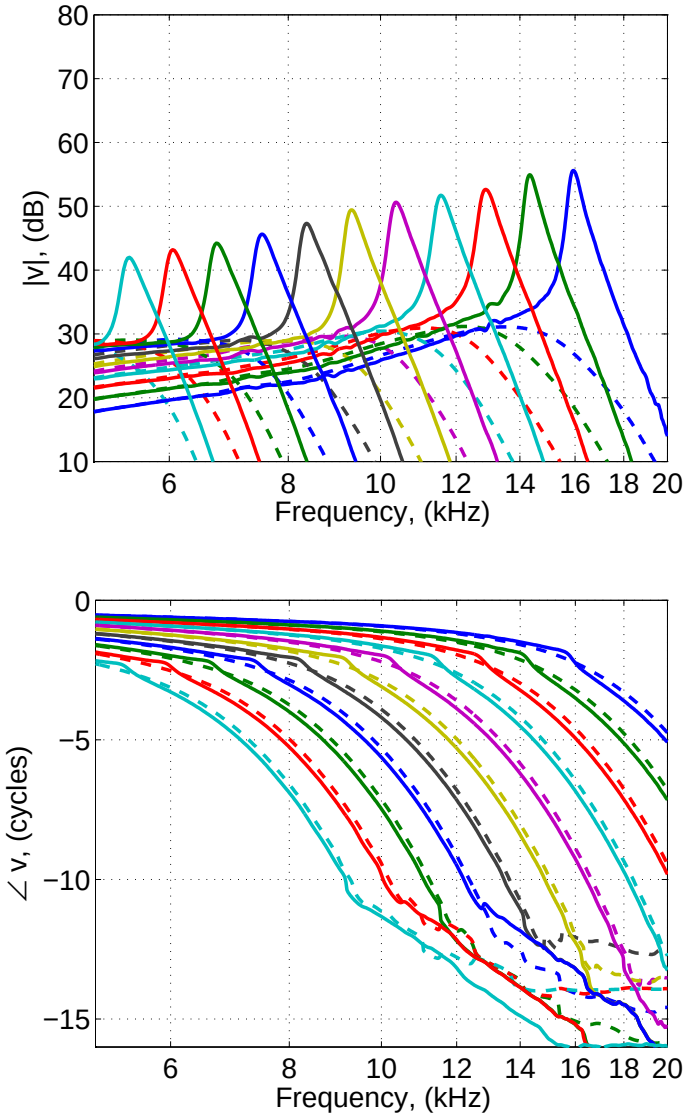

Figure 27: Response of the whole coupled active and passive cochlea using full 3D fluid coupling with realistic cochlear chamber values. Response at x=10.2 mm, 9.7 mm, 9.3 mm, 8.8 mm, 8.3 mm, 7.8 mm, 6.8 mm, 6.3 mm, 5.8 mm and 5.3 mm.

B State space model: Coupled stability

The state space formulation rearranges the discrete set of micromechanical elements taking also in account the effect of the fluid coupling. By the use of this formulation the stability of the coupled cochlea can be assessed. This is of quite importance, as it can be the case that even when the isolated micromechanics of each element are stable, the coupled response results to be unstable. The formulation here introduced has been adapted from [24, 25].

The OC dynamics of each mass are defined as

$$p_A - p_{OHC} = m_1\ddot{w}_{BM} + k_1 w_{BM} + k_2(w_{BM} - w_{RL}),$$

$$p_{OHC} = m_2\ddot{w}_{RL} + k_2(w_{RL} - w_{BM}) + k_3(w_{RL} - w_{TM} + k_5 w_{RL}),$$

$$0 = m_3\ddot{w}_{TM} + k_3(w_{TM} - w_{RL}) + k_4 w_{TM}.$$

p_{OHC} is described using the actuator of Appendix C

$$\frac{P_{OHC}}{w_{ST}} = \frac{\gamma k_A}{1 + j\omega/\omega_A}, \tag{B.1}$$

where

$$k_A = g'\varepsilon_3 Z_m V_0 G_a, \qquad \omega_A = R_m C_m. \tag{B.2}$$

p_{OHC} can then be expresses as

$$p_{OHC} = \omega_A \left(-p_{OHC} + \gamma k_A w_{ST}\right). \tag{B.3}$$

The state space form for each micromechanical element of the cochlea is

$$\dot{\mathbf{x}}_n(t) = \mathbf{A}_n \mathbf{x}_n(t) + \mathbf{B}_n p_n(t) \tag{B.4}$$

$$\dot{\mathbf{w}}_n(t) = \mathbf{C}_n \mathbf{x}_n(t), \tag{B.5}$$

where $\dot{\mathbf{x}}_n(t)$ is the vector of state variables associated with the n_{th} micromechanical model. At a given time instant, these matrices are defined as

$$\dot{\mathbf{x}}_n = \begin{bmatrix} \dot{x}_1 \\ \dot{x}_2 \\ \dot{x}_3 \\ \dot{x}_4 \\ \dot{x}_5 \\ \dot{x}_6 \\ \dot{x}_7 \end{bmatrix} = \begin{bmatrix} \dot{w}_{BM} \\ \dot{w}_{RL} \\ \dot{w}_{TM} \\ \ddot{w}_{BM} \\ \ddot{w}_{RL} \\ \ddot{w}_{TM} \\ \dot{p}_{OHC} \end{bmatrix}, \quad \mathbf{B}_n = \begin{bmatrix} 0 \\ 0 \\ 0 \\ 1/m_1 \\ 0 \\ 0 \\ 0 \end{bmatrix}, \quad \mathbf{C}_n = \begin{bmatrix} 1 & 0 & 0 & 0 & 0 & 0 & 0 \end{bmatrix}, \tag{B.6}$$

$$\mathbf{A}_n = \begin{bmatrix} 0 & 0 & 0 & 1 & 0 & 0 & 0 \\ 0 & 0 & 0 & 0 & 0 & 1 & 0 \\ 0 & 0 & 0 & 0 & 0 & 0 & 1 \\ -(k_1+k_1)/m_1 & k_2/m_1 & 0 & 0 & 0 & 0 & -1/m_1 \\ k_2/m_1 & -(k_2+k_3+k_5)/m_2 & k_3/m_2 & 0 & 0 & 0 & 1/m_2 \\ 0 & k_3/m_3 & -(k_3+k_4)/m_3 & 0 & 0 & 0 & 0 \\ 0 & \gamma k_A \omega_A & -\gamma k_A \omega_A & 0 & 0 & 0 & -\omega_A \end{bmatrix}. \tag{B.7}$$

B.1 Poles of the organ of Corti model

The poles of the organ of Corti model can be obtained by performing the eigenvalue decomposition of the state space matrix, defined in Eq. B.7. Fig. 28 shows the poles for the mechanical system at 5.75 mm from the base for different active gains, between γ=0 and γ=1.

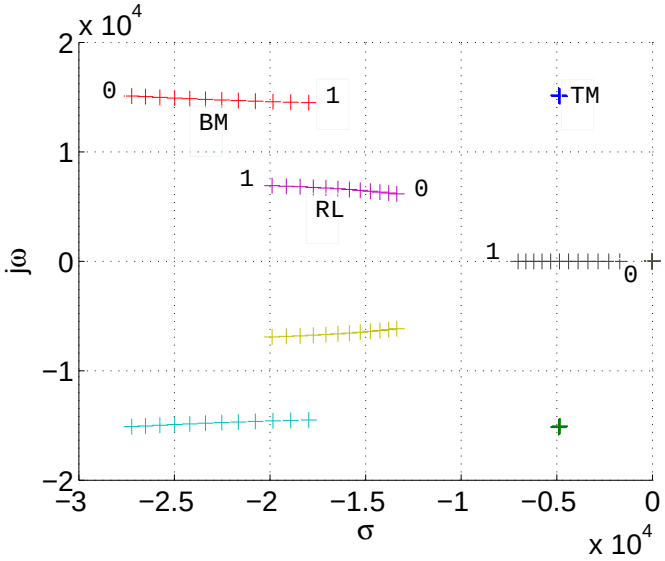

Figure 28: s plane plot of the poles of the isolated dynamics of the organ of Corti, at $x = 5.75mm$ for different OHC gains.

It is possible to observe how the poles move in a direction almost perpendicular to the $j\omega$ axis for different amplification levels, as previously shown by Shera[26], so that the OHC feedback forces not significantly alter the natural frequencies of the cochlear partition. This causes that the zero crossings of the impulse response remain almost invariant with the amount of feedback gain used, similarly to what have been found in measurements in live Guinea pig cochleas[20].

B.2 Poles of the coupled cochlea

The matrices defining each uncoupled micromechanical element can be rearranged together to form matrices containing the whole set of micromechanical elements

$$\dot{\mathbf{x}}(t) = \mathbf{A}_E\mathbf{x}(t) + \mathbf{B}_E p(t) \tag{B.8}$$

$$\dot{w}(t) = \mathbf{C}_E\mathbf{x}(t), \tag{B.9}$$

where the matrices which are block diagonal, are defined as

$$\mathbf{A}_E = \begin{bmatrix} \mathbf{A}_1 & 0 & \dots & & \\ 0 & \mathbf{A}_2 & & & \\ \vdots & & \ddots & & \vdots \\ & & & \mathbf{A}_{N-1} & 0 \\ & & \dots & 0 & \mathbf{A}_N \end{bmatrix}, \mathbf{B}_E = \begin{bmatrix} \mathbf{B}_1 & 0 & \dots & & \\ 0 & \mathbf{B}_2 & & & \\ \vdots & & \ddots & & \vdots \\ & & & \mathbf{B}_{N-1} & 0 \\ & & \dots & 0 & \mathbf{B}_N \end{bmatrix}$$

$$\mathbf{C}_E = \begin{bmatrix} \mathbf{C}_1 & 0 & \dots & & \\ 0 & \mathbf{C}_2 & & & \\ \vdots & & \ddots & & \vdots \\ & & & \mathbf{C}_{N-1} & 0 \\ & & \dots & 0 & \mathbf{C}_N \end{bmatrix}. \tag{B.10}$$

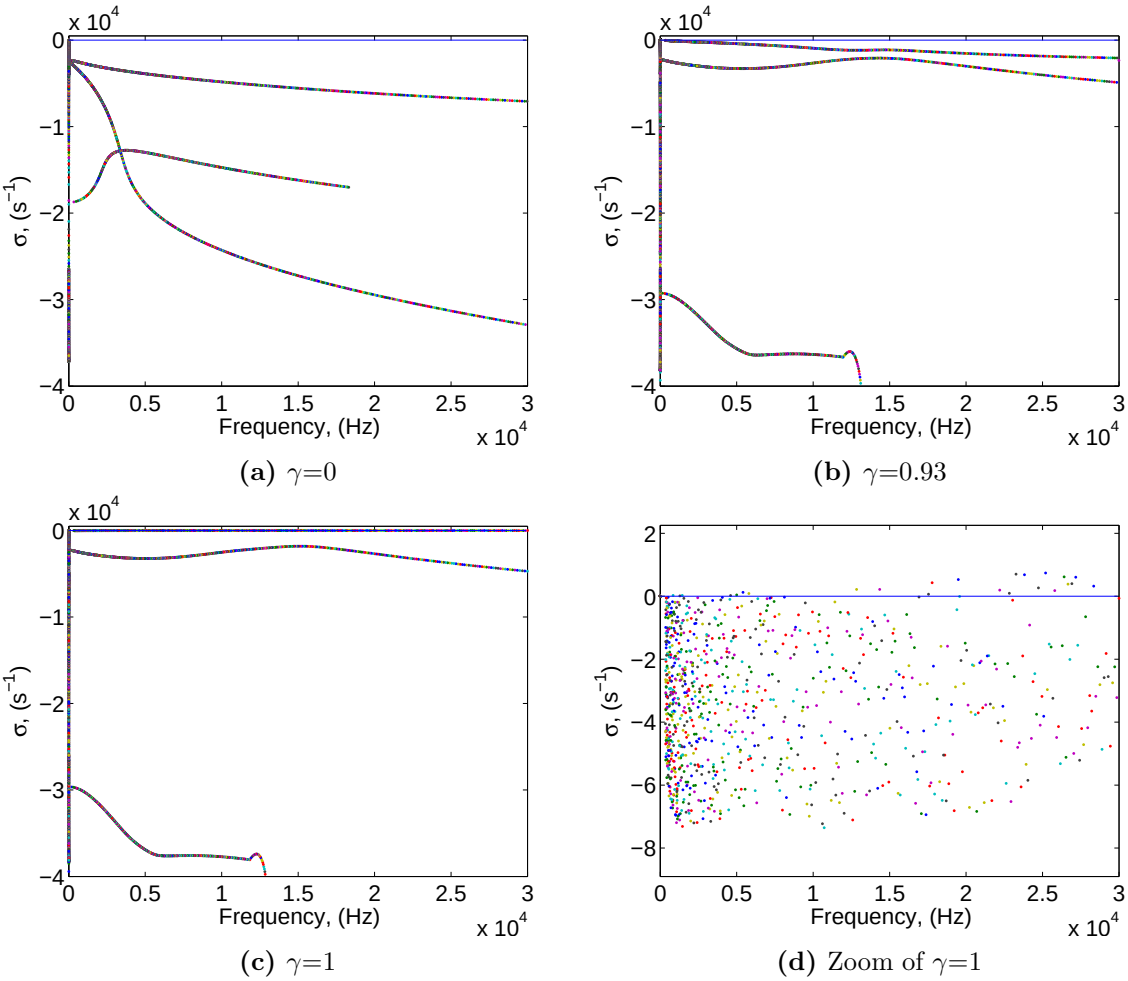

(a) γ=0 **(b)** γ=0.93

(c) γ=1 **(d)** Zoom of γ=1

Figure 29: Poles of the coupled cochlea for different OHC gain configurations.

The pressure of vectors along the BM can also be expressed as

$$\mathbf{p}(t) = \mathbf{G}\ddot{\mathbf{w}}(t) + \mathbf{G}\mathbf{q}, \tag{B.11}$$

where $\mathbf{G} = \mathbf{Z}_{FC}/j\omega$, $\ddot{\mathbf{w}} = j\omega\mathbf{v}$ and $\mathbf{q} = j\omega\mathbf{v}_S$. For the case of 1D fluid coupling $\mathbf{Z}_{FC} = \mathbf{Z}_L$ and for the case of 3D fluid coupling $\mathbf{Z}_{FC} = \mathbf{Z}_L + \mathbf{Z}_N$. Using Eq. B.9 the vector of pressures $\mathbf{p}$ can be rearranged into

$$\mathbf{p}(t) = \mathbf{G}\mathbf{C}_E\dot{\mathbf{x}}(t) + \mathbf{G}\mathbf{q}(t). \tag{B.12}$$

Substituting into Eq. B.8 leads to an state space expression for the coupled cochlea, expressed as

$$\dot{\mathbf{x}}(t) = \mathbf{A}\mathbf{x}(t) + \mathbf{B}\mathbf{u}(t), \tag{B.13}$$

where

$$\mathbf{A} = \left[\mathbf{I} - \mathbf{B}_E\mathbf{G}\mathbf{C}_E\right]^{-1}\mathbf{A}_E, \tag{B.14}$$

$$\mathbf{B} = \left[\mathbf{I} - \mathbf{B}_E\mathbf{G}\mathbf{C}_E\right]^{-1}\mathbf{B}_E, \tag{B.15}$$

$$\mathbf{u} = \mathbf{F}^{-1}\mathbf{q}. \tag{B.16}$$

The matrix $\mathbf{A}$ is called the system matrix and it determines the transient response of the system. The eigenvalues of $\mathbf{A}$ are the poles of the system's transfer function and hence they can be used to determine the stability of the coupled cochlea. The real parts of every single eigenvalue must be negative if the transient response is to decay away, so that the system is stable.

Figure 29 shows the positions of the poles of the model with different gain configurations, where the value of γ refers to the point where the open loop response HG_{SO} crosses the negative real axis. It is important to say that the state space analysis shows a pole with 0 real part at 0 Hz.

C Simplified OHC model

C.1 Formulation

The following assumptions are performed here with respect to the OHC model of Ramamoorhty *et al.*[1]:

- A single row of OHC is used instead of three rows as in the original model.
- No longitudinal coupling on the BM. The current flowing on a single OHC is due to the current of the OHC itself and not by potential differences on any of the scales.

By modifying Eq. 21 of[1] p_{OHC} can be defined as

$$p_{OHC} = k_2(w_{RL} - w_{BM}) + \gamma\varepsilon_3\phi_{OHC}, \tag{C.1}$$

where γ allows us to select the level of active amplification, ε_3 represents the electromechanical coupling coefficient and ϕ_{OHC} represents the voltage across the OHC. As no longitudinal coupling is modelled here, this last quantity is defined as the product of the current through the OHC, I_{OHC}, by the OHC electrical impedance, Z_m,

$$\phi_{OHC} = Z_m I_{OHC}, \tag{C.2}$$

where $Z_m = (1/R_m + j\omega C_m)^{-1}$. I_{OHC} is proportional to the steady voltage at the OHCs, V_0, to the conductance function, G_a, which varies with the position along the cochlea, and to the stereocillia displacement, $w_{ST} = w_{TM} - w_{RL}$

$$I_{OHC} = V_0 G_a w_{ST}, \tag{C.3}$$

where G_a is defined by Ramamoorthy *et al.*[1], based on numerical experiments, as

$$G_a = G_a(0)\left(-10^5x^3 + 5.910^3x^2 - 109x + 1\right)e^{-150x} \tag{C.4}$$

p_{OHC} is then defined as

$$p_{OHC} = k_2(w_{BM} - w_{RL}) + \gamma\varepsilon_3 Z_m V_0 G_a w_{ST};$$

$$p_{OHC} = k_2(w_{BM} - w_{RL}) + H w_{ST}, \tag{C.5}$$

where H is defined as

$$H = \frac{\gamma g'\varepsilon_3 Z_m V_0 G_a}{1 + j\omega R_m C_m} = \frac{\gamma g_H}{1 + \frac{j\omega}{\omega_{OHC}}}, \tag{C.6}$$

where $\omega_{OHC} = (R_m C_m)^{-1}$, and g_H is defined as the MET overall gain

$$g_H = g'\varepsilon_3 Z_m V_0 G_a. \tag{C.7}$$

The value of the parameters used in the formulation, obtained from Ramammorthy *et al.*[1] are presented in Table. 8.

Table 8: Value for the electrical parameters used in the OHC compensator.

Element	Value	Units
ε_3	$(-8 \cdot 10^{-6} \cdot 10^{-5}x)$	N/m/mV
$1/R_m$	$5100_{\text{(base) to}}\ 360\ _{\text{(apex)}}$	μS/m
C_m	$1800\ _{\text{(base) to}}\ 4200\ _{\text{(apex)}}$	nF/m
$G_a(0)$	$5.447{\cdot}10^6$	S/m^2
V_0	$150 - 1000x$	mV
$\omega_{OHC}/2\pi$	$450_{\text{(base) to}}\ 13.7\ _{\text{(apex)}}$	Hz

C.2 Controller dynamics

The required gain to apply to H in order to obtain an active amplification, g', is obtained

$$g' = \frac{1}{\Re\{H(fp)G_{SO}(fp)\}}, \tag{C.8}$$

where fp represents the point of the response which its phase is -0.5 cycles and hence will be closer to the (-1,0) point. The aspect of g' is shown in Fig. 30. The magnitude and

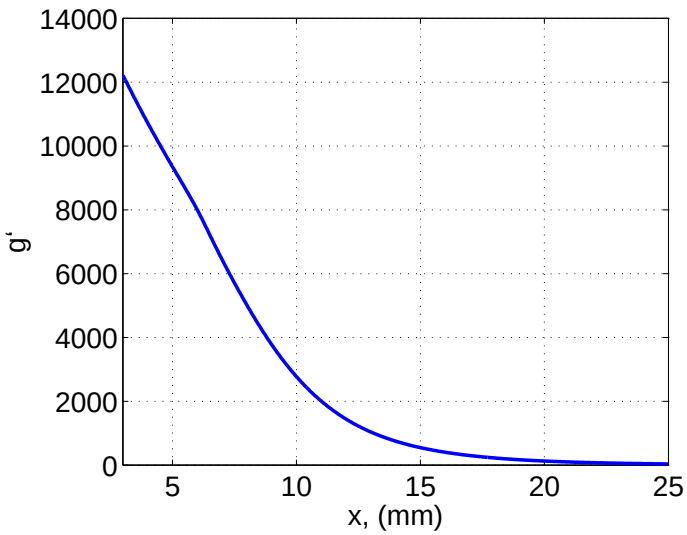

Figure 30: Gain function in order to place the response of HG_{SO} close to (-1,0).

phase of the controller H against position along the cochlea and against frequency can be observed in Fig. 31. The response at the positions of the analysis of Section 7 are shown in Fig. 32.

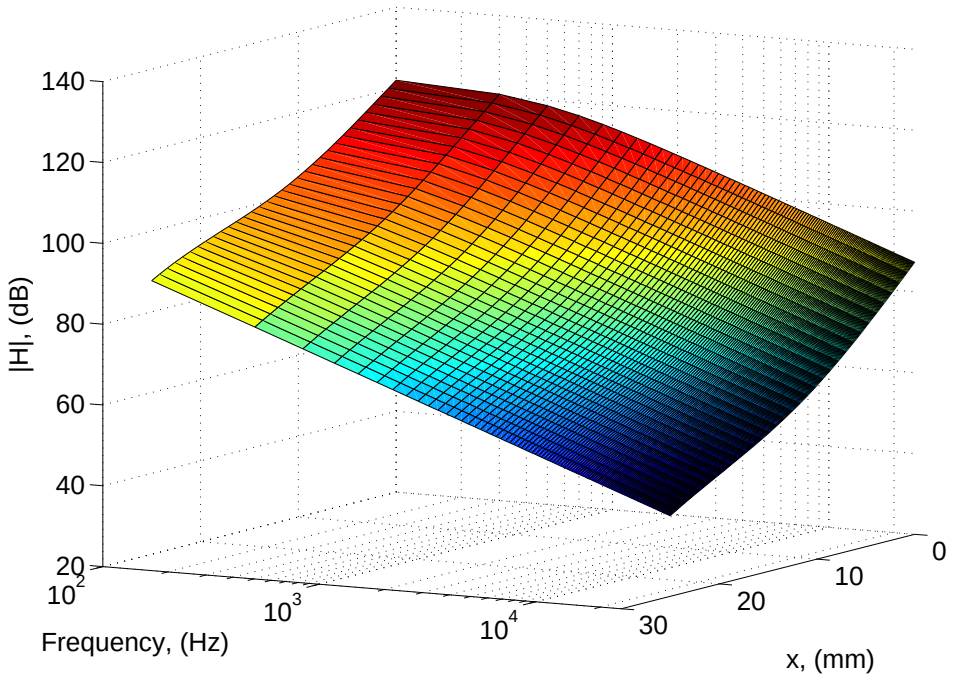

(a) Controller magnitude response against BM position and frequency.

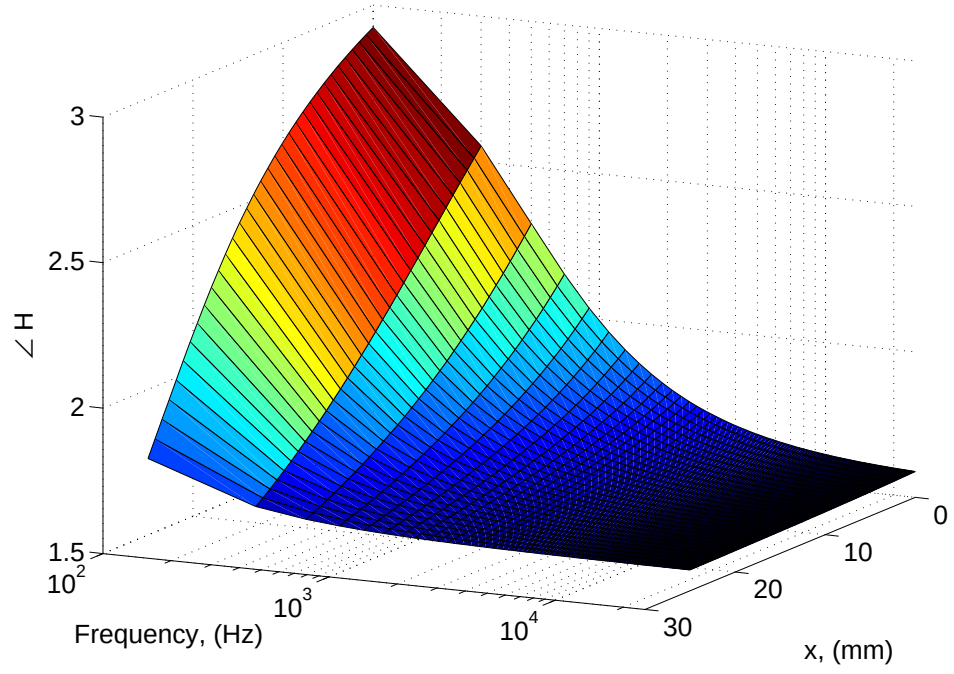

(b) Controller phase response against BM position and frequency.s

Figure 31: Controller dynamics.

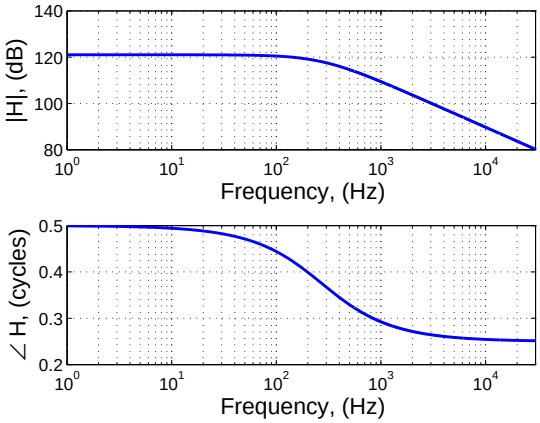

(a) 5.75 mm

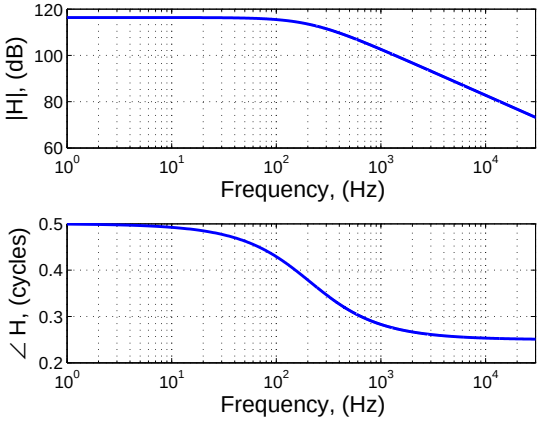

(b) 8.75 mm

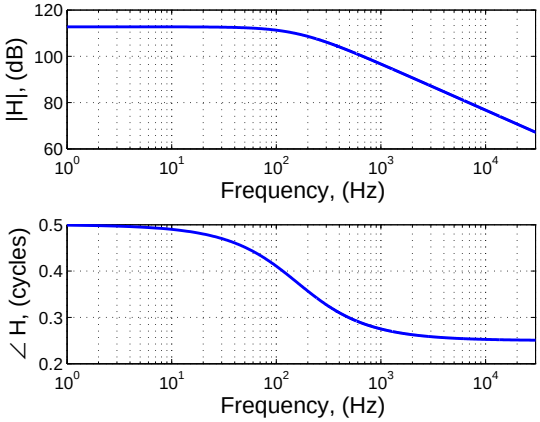

(c) 11.75 mm

Figure 32: Responses of the controller H at different positions along the length of the cochlea.

D The coupling factor for piezoelectric activity in outer hair cells

D.1 Introduction

The electromechanical properties of the outer hair cells in the ear are central to their action as part of the cochlear amplifier, which significantly amplifies the motion of the basilar membrane. These electromechanical properties are defined in different ways in different parts of the literature and the purpose of this report is to compare these different formulations so that comparisons can be made of the assumed outer hair cell parameters across different models. Of particular interest is the nondimensional coupling factor for outer hair cell models and how the magnitude of this affects the representation of the outer hair cell in cochlear models in which the outer hair cell is coupled to the organ of Corti.

D.2 Piezoelectric equations

The constitutive equation of a piezoelectric material can be expressed as[27]

$$D = \varepsilon^T + dT \tag{D.1}$$

$$S = dE + s^E T \tag{D.2}$$

where D is the charge per unit area, E is the electric field, T is the stress and S the strain. The dielectric permittivity under constraint stress is denoted ε^T, s^E is the inverse of the Young's modulus under constant electric field and d is the piezoelectric constant for the material.

The electromechanical coupling factor for the piezoelectric material, which is a nondimensional number between 0 and 1 that quantifies the conversion of mechanical to electrical energy and vice versa, is given by

$$k^2 = \frac{d^2}{s^E \varepsilon^T}. \tag{D.3}$$

Equations D.1 and D.2 are simplifications of a full matrix set of equations in the general case that assume that the electric field and strain are only measured in a single direction. If both of these are aligned with the poling direction of the piezoelectric material, along which the electric dipoles are aligned, then the corresponding piezoelectric constant is denoted d_{33}. If the electric field is aligned with the poling direction but the strain is measured in a direction at right angles, the corresponding piezoelectric constant is denoted d_{31}. Piezoelectric materials such as lead zirconate titanate (PZT) have significant values for both d_{33} and d_{31} and a electromechanical coupling coefficient, k^2, of the order of 0.7.

It is convenient to describe the piezoelectric models for the OHC within the framework of a two port network, as shown in Fig. 33, which links the overall electrical variables of charge, q, and voltage, v, to the mechanical variables of displacement, w, and force, f. For small excitations the electrical and mechanical variables can be defined as perturbations on larger mean values and the relationships between these variables becomes linear. There are a number of ways in which the relationship between the electrical and mechanical variables can be expressed. Initially we choose a representation that is common for engineering piezoelectric actuators [27] and express q and w as functions of v and f, so that in matrix

form

$$\begin{bmatrix} q \\ w \end{bmatrix} = \begin{bmatrix} C_P & d_P \\ d_P & 1/K_P \end{bmatrix} \begin{bmatrix} v \\ f \end{bmatrix}. \tag{D.4}$$

Where C_P is the free capacitance, i.e. with no applied force, K_P is the short circuit stiffness, i.e. with the applied voltage set to zero and d_P is the piezoelectric constant, which is equal to both the charge per unit force when the voltage is zero and the displacement per unit voltage when the force is zero, since the action is assumed to be reciprocal. The validity of the reciprocity condition for the outer hair cells has been examined by Dong *et al.*[28] and found to be satisfied.

An advantage of the formulation in Eq. D.4 is that while C_P and K_P depend on the geometry and dimensions of the OHC, d_P is a material property of the piezoelectric, independent of size and shape.

The displacement of the transducer per unit applied voltage will vary depending on the mechanical loading that it is subject to. With no mechanical loading, so that if f is zero in equation Eq. D.4, then w/v, is, by definition, equal to d_P. If, however, we assume that a force is applied such that the charge generated exactly cancels the charge due to voltage, then q in Eq. D.4 is equal to zero, so that the force must be

$$f|_{q=0} = -\frac{C_P}{d_P} v, \tag{D.5}$$

$$\frac{w}{v}|_{q=0} = d_P \left(1 - \frac{C_P}{d_P^2 K_P}\right). \tag{D.6}$$

If we define the nondimensional coupling factor for the transducer as being

$$k_P^2 = \frac{d_P^2 K_P}{C_P}, \tag{D.7}$$

then Eq. D.2 becomes

$$\frac{w}{v}|_{q=0} = d_P \frac{k_P^2 - 1}{k_P^2}. \tag{D.8}$$

If this coupling factor is comparable with unity, then Eq. D.8 will be significantly different from d_P and the displacement per unit voltage will be very dependent on the electrical and mechanical conditions imposed on the transducer. If the coupling factor in Eq. D.7 is small compared to unity, however, then the displacement will not be dependent on the electrical and mechanical conditions imposed on the transducer and can be assumed to be constant in models where the OHC is coupled to the dynamics of the organ of Corti. It is thus important to estimate the magnitude of the nondimensional coupling factor given by Eq. D.7 in the case of the OHC, since it will have an important bearing on the complexity of the electrical model that needs to be used in a coupled cochlear model.

If the transducer was made of a solid element of piezoelectric material, of length l and cross sectional area A, and the electrical and mechanical variables are measured along the poling axis, the piezoelectric constant, d_P, would be equal to d_{33}. The capacitance, C_P, would then be equal to $\varepsilon^T A/l$, where ε^T is the dielectric permittivity defined in Eq. D.1 and the stiffness, K_P, would be equal to $A/s^E l$, where $(s^E)^{-1}$ is the Young's modulus in Eq. D.1. In this case the quantity k_P^2 in Eq. D.8 is equal to the electromechanical coupling

factor for the piezoelectric material, k^2, as defined in Eq. D.3[27].

In the case of the outer hair cell, however, the geometry is more similar to an open cylinder, as shown in Fig.33. The piezoelectric constant, d_P, would be equal to d_{31}, for the piezoelectric material in this case. The outer hair cells are not entirely made up of piezoelectric material, which is the protein prestin in this case, but if we assume that the capacitance of the outer hair cell is dominated by the piezoelectric material then it can be approximated by $\varepsilon^T A_C t_C$, where A_C is the effective area of the capacitor, which is $2\pi rl$ for the cylinder in Fig.33, and t_c is its thickness, which is Δr for this cylinder, so that

$$C_P = \frac{2\pi r \varepsilon^T l}{\Delta r}. \tag{D.9}$$

Similarly, if the stiffness of OHC, K_P is dominated by the piezoelectric material then it is given by $A_K/S_E l_K$, , where A_K is the cross sectional area, which is approximately equal to $2\pi r\Delta_r$ for the cylinder in Fig. 33, and l_K is the length, equal to l for this cylinder, so that

$$K_P = \frac{2\pi r \Delta_r}{s^E l}. \tag{D.10}$$

The coupling factor for a cylindrical transducer, which has an electromechanical coupling factor of the piezoelectric material, k^2, is now equal to

$$\frac{d_P^2 K_P}{C_P} = k^2 \left(\frac{\Delta r}{l}\right)^2. \tag{D.11}$$

So, if the capacitance and stiffness of the outer hair cell are primarily determined by the properties of the piezoelectric material, which must have a material electromechanical coupling factor, k^2, which is less than one, the overall coupling factor, when acting as a transducer, must be small if the OHC is long compared with the thickness of the cell wall, so that $\left(\frac{\Delta r}{l}\right)^2$ is much less than unity.

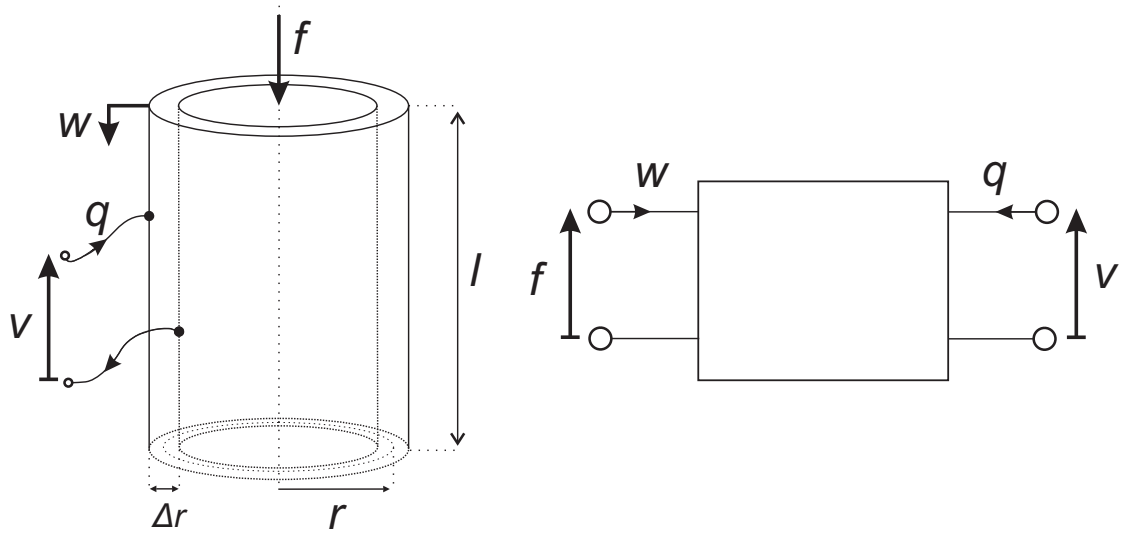

Figure 33: An idealisation of a cylindrical outer hair cell subject to a force, f, and being compressed by a displacement, w, when driven by a charge, q, generating a voltage across the cell wall of v, and a the two port representation of this.

D.3 Parameter values of the outer hair cells

The piezoelectric equations are expressed in different ways by different authors, so some transformation is needed in order to compare the parameter values, Iwasa [29] emphasises that the parameters are non-linear functions of the membrane potential across the outer hair cell, as also discussed by Deo and Grosh[30], but they estimate that the largest value of the linearised parameters for the outer hair cell is about

$$C_P \approx 3.7 \cdot 10^{-11} \text{ F}, \quad K_P = 8 \cdot 10^{-3} \text{ Nm}^{-1},$$

so that

$$d_P \approx 2 \cdot 10^{-5} \quad \text{mv}^{-1} \text{ or } \text{CN}^{-1}$$

The the coupling factor for this model can be directly calculated as

$$\frac{d_P^2 K_P}{C_P} \approx 0.086,$$

although Iwasa [29] chooses, in his Fig. 3, to plot k_P rather than k_P^2 in our notation. It is noteworthy that the piezoelectric constant estimated for the outer hair cell, 20μm/V, is about a factor of 10^5 greater than PZT, for which d_3, is about 150 pm/V, and a factor of about 10^6 greater than the polyvinylidene fluoride (PVDF), for which d_S, is about 15 pm/V. The coupling factor of the outer hair cell, in equation (3.2), however, is much less than the coupling factor of a solid piezoelectric device made of PZT, for which k^2 would be about 0.7, or PVDF, for which k^2 would be about 0.1, since K_P/C_P is significantly smaller for the OHC than in the PZT case.

Ramamoorhty *et al.* choose to express their linearised piezoeletric equations, 21 and 22 of their paper, in a form equivalent to

$$f = K_{OHC} w_{ST} + \varepsilon_3 v \tag{D.12}$$

$$q = -\varepsilon_3 w_{st} + C_m v. \tag{D.13}$$

Where the symbols above have been used for force, f, displacement, w, voltage, v and charge q, and the low frequency approximation has been taken for their Z_m. Those equations may be re-written, in the same form as Eq. D.4, as

$$q = \left(C_m - \frac{\varepsilon_3^2}{K_{OHC}} \right) v + \frac{\varepsilon_3}{K_{OHC}} f \tag{D.14}$$

$$w = \frac{\varepsilon_3}{K_{OHC}} v + \frac{1}{K_{OHC}} v \tag{D.15}$$

The values of the parameters used by Ramamoorthy *et al.*[1] at the base of the cochlea are ε_3 equal to $-8 \cdot 10^{-6}$ Nm $^{-1} mV^{-1}$, C_m equal to $1.8 \cdot 10^{-6}$ Fm^{-1} and K_{OHC} equal to $7.6 \cdot 10^3$ Nm^{-2}, which are all per unit length.

The parameters corresponding to C_M and K_{OHC} in Eqs. D.14 and D.15 thus cannot be directly compared to those above, but d_P, which equals ε_3/K_{OHC} is independent of and directly comparable to the piezoelectric constant, above, and has a value of about 10^{-9} m V^{-1}, which is much smaller than that assumed by Iwasa[29]. The length-dependence of C_P

and K_P are cancelled out, however, when the overall coupling coefficient is calculated in this case as

$$\frac{d_P^2 K_P}{C_P} = \frac{\varepsilon_3^2}{K_{OHC}(C_m - \varepsilon_3^2/K_{OHC})} \approx \quad 4.6 \cdot 10^{-9},$$

which is much lower than the value described by Iwasa[29].

Maoiléidigh and Jülicher[31] express the piezoeletric relationship for the outer hair cell model in the form

$$\begin{bmatrix} v \\ f \end{bmatrix} = \begin{bmatrix} 1/C_{ohc} & p \\ p & K_{ohc} \end{bmatrix} \begin{bmatrix} q \\ w \end{bmatrix}. \tag{D.16}$$

Where again the symbols for voltage, force, charge and displacement are as used above, and the sign convention for w is opposite to the one they use for displacement. This matrix equation can be inverted to give one in the same form as Eq. D.4 above, so that

$$\begin{bmatrix} q \\ w \end{bmatrix} = \left(\frac{K_{ohc}}{C_{ohc}} - p^2 \right) \begin{bmatrix} K_{ohc} & -p \\ -p & 1/C_{ohc} \end{bmatrix} \begin{bmatrix} v \\ f \end{bmatrix}. \tag{D.17}$$

With the values used by Maoiléidigh and Jülicher[31] , of p equal to $1.6{\cdot}10^4$ Vm^{-1} (Table I), C_{ohc} equal to 2.0 10^{-11} F, (Table I), and K_{ohc} equal to 10^{-2} Nm^{-1},(Table V), then the equivalent value of d_p is about $1.2{\cdot}10^{-4}$ mV^{-1}, rather larger than that assumed by Iwasa[29]. The coupling factor for the outer hair cell model in their case is thus given by

$$\frac{d_P^2 K_P}{C_P} = \frac{p^2 C_{ohc}}{K_{ohc}} \approx \quad 0.5,$$

which is significantly larger than that assumed by Iwasa [29] or Ramamoorhty *et al.*[1].